



Stockholm
University

Master Thesis

Degree Project in
Climate Science 45 hp

Mid- to Late Holocene mineral deposition and peat decomposition in the Faroe Islands: geochemistry, mineralogy and tephra

Andreas Nylund



Stockholm 2022

Department of Geological Sciences
Stockholm University
SE-106 91 Stockholm

Abstract

The climate of the Faroe Islands is heavily determined by variations in important large-scale climate patterns of the North Atlantic Ocean like the AMOC and NAO. This makes the Faroe Islands highly interesting in a paleoclimatic context, with the possibility of tracing past variation in these patterns and assessing landscape impact from any change. Previous paleoclimatic studies on the Faroe Islands have been mostly focused on biological proxies and/or lacustrine sediments. To improve the spatial coverage and the range of proxies and archives used, a peat core representing the last ~8000 years from the mire complex of Mýrarnar is examined with the aim to reconstruct past variation in mineral deposition and peat decomposition. This is done through interpreting variations in elemental geochemistry determined by XRF analysis, mineralogy inferred from XRD, SEM-EDS and ATR-FTIR analyses, ash content and bulk density throughout the peat sequence. The degree of peat decomposition in the studied sequence generally increases with time, indicating that the Holocene climate of the Faroe Islands became gradually drier. Eight mineral deposition events are identified by increased lithogenic element and mineral input, with peaks dated to 7790, 5740, 4440, 4130, 3740, 2800, 1960 and 820 cal yr BP. At least three of these events have considerable contents of tephra, while the character of the other events remains unknown. It is possible that the uncharacterized events represent further tephra deposition. They could also represent storm events where remobilization of previously deposited tephra could make up much of the lithogenic input. To improve the paleoclimatic interpretation of the Mýrarnar lithogenic input record, further characterization of the mineral deposition events and future directions on differentiating climatic and volcanic signals are proposed.

Table of Contents

1. Introduction	5
1.1. Project Aims	7
2. Background	8
2.1. Geographical Setting	8
2.1.1. Geology	8
2.1.2. Meteorology	8
2.2. Governing Climate Mechanisms	10
2.3. Holocene Climate in the Faroe Islands	11
2.3.1. Early to Mid-Holocene Climate	11
2.3.2. Human Colonisation	12
2.3.3. Tephra Deposition	13
2.4. Mire Development	13
2.4.1. Peat Accumulation and Mire Development	13
2.4.2. Peat in the Faroe Islands	14
2.5. Geochemical and Physical Proxies in Peat Environmental Reconstructions	15
2.5.1. Peat as an Environmental Archive	15
2.5.2. Methods in Peat Paleoenvironmental Reconstructions	15
3. Study Area	18
4. Methods	19
4.1. Sampling	19
4.1.1. Field Sampling	19
4.1.2. Sub-sampling	19
4.2. Analyses	20
4.2.1. Radiocarbon Dating, Age-Depth Model and Growth Rate	20
4.2.2. Bulk Density, Core Alignment and Ash Content	20
4.2.3. Elemental Geochemistry	20
4.2.6. Attenuated Total Reflection Fourier Transform Infrared (ATR-FTIR) Spectroscopy	21

4.2.7. X-Ray Diffraction (XRD) Mineral Analysis	21
4.2.8. Scanning Electron Microscope – Energy Dispersive Spectroscopy (SEM-EDS) Analysis	22
4.3. Statistical Analyses	22
5. Results	23
5.1. Chronology	23
5.2. Peat Properties	24
5.2.1. Visual Stratigraphy	24
5.2.2. Bulk density, PAR, Ash Content and AAR	24
5.3. Elemental Geochemistry and PCA	26
5.4. Mineral Composition	29
5.4.1. ATR-FTIR	29
5.4.2. XRD	30
5.4.3. SEM-EDS	31
6. Discussion	32
6.1. Deposit Characterisation	32
6.2. Relationship between Geochemical Tools	34
6.3. Proxy Interpretation	34
6.3.1. Elemental Data	34
6.3.2. Spectral Data	38
6.4. Proxy Synthesis- Paleoenvironmental Summary	39
6.5. Implications and Future Prospects	42
Conclusion	45
Acknowledgements	45
References	46
Appendix	59
A. Age-Depth Model	59
B. Individual Element Profiles	60
C. XRD-Diffractograms	62

1. Introduction

The North Atlantic Ocean is one of the few regions in the world where robust warming is not inferred from climate model projections (Lee et al., 2021). This is partially attributed to the projected and observed weakening of the Atlantic meridional overturning circulation (AMOC) (Fox-Kemper et al., 2021; Caesar et al., 2021). The AMOC is a system of ocean currents responsible for much of the poleward transport of heat from lower latitudes and is as such a major component in the North Atlantic climate variability (Buckley and Marshall, 2016; Marshall et al., 2001; Kuhlbrodt et al., 2007). While the AMOC is deemed very likely to decline in the 21st century, the inter-model projection spread is high and there is low confidence in the rate and magnitude of change (Fox-Kemper et al., 2021; Reintges et al., 2017). Another major mode of climate variability in the region is the North Atlantic Oscillation (NAO, a regional counterpart to the Northern Annular Mode), which describes atmospheric pressure differences over the North Atlantic Ocean (Hurrell, 1995; Gillet et al., 2003). The fluctuations of the NAO exert major influence on precipitation and temperature patterns and are linked to the strength and trajectory of westerly winds, jet streams and cyclonic storms (Hurrell and Van Loon, 1997; Feser et al., 2015; Woolings and Blackburn, 2012; Deser et al., 2017; Olsen et al., 2012). The development of the NAO with global warming is uncertain and exhibit large spread in model projections (McKenna and Maycock, 2021; Deser et al., 2017). Both the AMOC and the NAO are instrumental in describing North Atlantic climate and both show large uncertainty in model projections. By extension, it is implied that the future North Atlantic climate development remains uncertain.

Increasing knowledge of the future North Atlantic climate is important for several reasons. The uncertainties in the future AMOC and NAO projections means that the timing and magnitude of any change in temperature, precipitation or storminess over the North Atlantic region are largely unknown (Lee et al., 2021). In extension, the same is true for potential climate change impacts on e.g., agriculture, infrastructure and drinking water availability. This means that the AMOC and NAO exert direct control over processes that could substantially affect the millions of people living in areas highly susceptible to North Atlantic climate variability. Improving the understanding of the future North Atlantic climate could aid in adapting human society to a changing world. Beyond the regional impacts, the ocean currents and cyclonic storm systems of the North Atlantic constitute key components of the global poleward heat transport, affecting the equator-pole temperature gradient (Zhang et al., 2004; Marshall et al., 2001). This presents one mechanism through which the North Atlantic climate state holds a significant influence on global circulation and climate. To improve knowledge of future climate change and its impacts in this region, the underlying mechanisms of the NAO and AMOC variability need to

be further understood to further constrain climate models (Reintges et al., 2017; McKenna and Maycock, 2021). One way of better understanding the future behaviour of North Atlantic climate change and its impacts on terrestrial systems where humans reside, is to improve knowledge on past variability and the response of terrestrial systems to change (e.g., Chen et al., 2021; Olsen et al., 2012; Caesar et al., 2021;). This can be done through exploring environmental proxies in paleoclimatic archives (Chen et al., 2021).

Located between Iceland, Scotland and Norway in the North-eastern Atlantic Ocean lies the remote and maritime Faroe Islands (~62°N, 7°W). In many ways, this mountainous and nearly treeless archipelago of 18 basaltic islands offers an excellent location for paleoclimatic studies in relation to terrestrial impacts of AMOC and NAO variability. Firstly, the Faroe Islands are situated at the interface of major oceanic currents that form key components of the AMOC, which means that any change in the AMOC (spatially and intensity) may have extensive impacts on the climate of the Faroe Islands. Secondly, the islands are situated near common North Atlantic storm tracks (Cappelen, 2020), which means that the landscape and climate is highly affected by the NAO. Lastly, the Faroe Islands are relatively unique in that the earliest estimate for human arrival is c. 5th century CE (Curtin et al., 2021; Church et al., 2013; Hannon et al., 2001; 2005). This means that for much of the Holocene, anthropogenic impacts were minimal. Given the islands' oceanic setting and relation to important large-scale North Atlantic climate patterns such as the AMOC and NAO, they can be considered highly susceptible to North Atlantic climate variability. In turn, this implies that paleoenvironmental archives located on the Faroe Islands may provide valuable information regarding the larger North Atlantic climate change and landscape impacts.

Terrestrial paleoclimatic Holocene reconstructions from the Faroe Islands have mostly been based on biological proxies (e.g., Jóhansen, 1985; Hannon et al., 2003; 2005; 2010; Hannon and Bradshaw, 2000; Curtin et al., 2019; 2021; Lawson et al., 2005; 2007; 2008) with only a few being based on physical or geochemical proxies (e.g. Olsen et al., 2010; Jessen et al., 2008; Andresen et al., 2006). Most of these studies are based on lake sediments and often focused on the Early Holocene or the time of human arrival. A notable gap within the existing Faroese paleoclimatic reconstructions is that of geochemical characterisation of peats, a well-established method in assessing past climates (e.g., Chambers et al., 2012; Chambers and Charman, 2004; Bindler, 2006; Blackford, 2000). This can be done by, e.g., studying minerals and elemental variation to infer mineral deposition events (e.g., Sjöström et al., 2020; 2022; Kylander et al., 2013; 2016; 2020; Martínez Cortizas et al., 2020) and peat decomposition (e.g., Martínez Cortizas et al., 2007; Biester et al., 2004).

Here, to address this gap, a peat core representing the last 8000 years from the Faroese mire complex of Mýrarnar is examined for a suite of geochemical and physical proxies. Peat cores from Mýrarnar

have previously been examined in a tephrochronological study by Persson (1968) and the heavy metal focused depositional studies of Shotyk et al. (2005a; 2005b). In this thesis, past Faroese environments is examined for mineral deposition events and peat decomposition using variations in bulk density, ash content and elemental geochemistry obtained through X-Ray fluorescence (XRF) techniques, which are complimented by mineralogy derived from X-Ray diffraction (XRD), scanning electron microscope – energy dispersive spectroscopy (SEM-EDS) and attenuated total reflection Fourier transform infrared (ATR-FTIR) spectroscopy. Mineral identification of peats with the latter is a novel approach and has so far only been applied in granitic settings (Martínez Cortizas et al., 2021). This means that this study is the first to use the technique in a basaltic setting.

1.1. Project Aims

The aim of this thesis is to improve the paleoclimatic coverage of the Faroe Islands, an archipelago with a paleoclimatically strategic location. This is attempted to be done by examining geochemical proxies in peat, which previously has been done to infer heavy metal deposition (Shotyk et al., 2005a; b) and tephrochronology (e.g. Wastegård, 2002; Wastegård et al., 2001; 2018) on the Faroe Islands. Here, geochemical techniques are used to reconstruct Faroese paleoclimatic variation in the hope of relating it to the wider climate of the North Atlantic region.

The main aim of this thesis is to reconstruct Holocene mineral deposition (elemental geochemistry, mineralogy and ash content) and peat decomposition (elemental geochemistry, bulk density and visual stratigraphy) at Mýrarnar. As a secondary objective, the drivers of the geochemical signal in the studied peat sequence will be explored.

2. Background

2.1. Geographical Setting

2.1.1. Geology

The Faroe Islands are located above a submarine ridge delineating the main North Atlantic Ocean from the marginal Norwegian Sea (Rasmussen, 1982), roughly 400 km north of mainland Scotland, 600 km west of Norway and 450 km southeast of Iceland (Figure 1). The archipelago of 18 main islands with several islets and skerries is characterised by a rugged topography with steeply inclining peaks ($>40^\circ$ slope common locally) reaching up to ~880 m a.s.l. from lower lying coasts (Rutherford and Taylor, 1982a). These features are the erosional remnants of a 3000-m thick plateau formed during the Paleogene from tholeiitic flood basalts, with interbedded pyroclastic tuffs and phenocrysts of plagioclase (Rasmussen and Noe-Nygaard, 1970; Rasmussen, 1982). Common minerals in the Faroese bedrock include plagioclase (mostly labradorite), pyroxenes (augite and pigeonite), olivine, magnetite and ilmenite (Holmes, 1918, Rasmussen and Noe-Nygaard, 1970). Despite being small in area, the Faroe Islands display some variation in the types of surficial deposits present owing to their mountainous relief. These have been described by Rutherford and Taylor (1982b) according to the Canadian system of soil classification (Canadian Soil Survey Committee, 1978). Regosols dominate steep slopes and exposed locations at higher altitudes, while gentle slopes are covered by podzols and cambisol and lower-lying depressions by gellisols. Histosols (at least 30% organic content) are found at most elevations in depressions, basins and poorly drained mountain plateaus, with peat being able to form up to 800 m a.s.l.. Coastal dunes are rare, but extensive aeolian deposits are widespread above 300 m a.s.l. (Christiansen, 1998; Humlum and Christiansen, 1998).

2.1.2. Meteorology

The Faroese climate has been described as `hyper-oceanic` (Crawford, 2000), characterised by cool summers and mild winters. The average monthly air temperature (1981-2010) in the coastal capital of Tórshavn is 11 °C for the warmest month of August and 3.6 °C for the coldest of February, with an annual mean of 6.8 °C (Cappelen, 2020). The islands are overall humid and wet, but the steep elevation differences induce a heterogeneity in precipitation following local topography. Coastal areas receive around 1000 mm of precipitation annually, while more central mountainous areas receive up to 3000 or even 4000 mm of precipitation annually (Cappelen, 2020). Part of this precipitation comes as snow, with snow covering coastal areas on average 44 days annually between 1961 and 1990 (Cappelen and Laursen, 1998). At higher altitudes local snow patches may persist for more than 300 days annually, as observed between 1999 and 2002 (Christiansen and Humlum, 2003). Precipitation varies according to

the season, with mean monthly precipitation between April and August (1981-2010) never exceeding 100 mm (lowest value 57.5 mm in June), a value which is well surpassed in the remaining months (highest value 157.7 mm in January) (Cappelen, 2020). The dominant wind direction in the region is from the south-west and the wind speeds, while generally high, vary both seasonally and spatially. The summer mean monthly wind speeds range from 4.5-6 m s⁻¹, while it is not irregular for those of winter to reach 10 m s⁻¹ with singular gusts reaching velocities of 70 m s⁻¹ (Cappelen and Laursen, 1998). In the eastward facing Tórshavn mean annual wind speed is 5.9 m s⁻¹ while the value for westernmost island of Mykines is 7.7 m s⁻¹ (Cappelen and Laursen, 1998). The strong winds, together with the grazing of sheep (Gimingham, 1964), help explain the nearly treeless and dominating grassy heath vegetation of the islands.

The steep and mountainous topography of the islands leads to relatively high climatic variations over short distances. The subpolar oceanic climate of the coasts gradually transitions into polar meteorological conditions at elevations exceeding 200 m.a.s.l., where the mean temperature of the warmest month does not exceed 10 °C (Christiansen and Mortensen, 2002). Periglacial activity, including patterned ground and sorted stripe formation, is present down to 150-300 m.a.s.l., constituting what is sometimes considered a southern marginal zone for periglacial activity (Humlum and Christiansen, 1998; Christiansen and Humlum, 2003). These boundaries shift up and down mountain slopes with time depending on the current climate (Humlum and Christiansen, 1998).

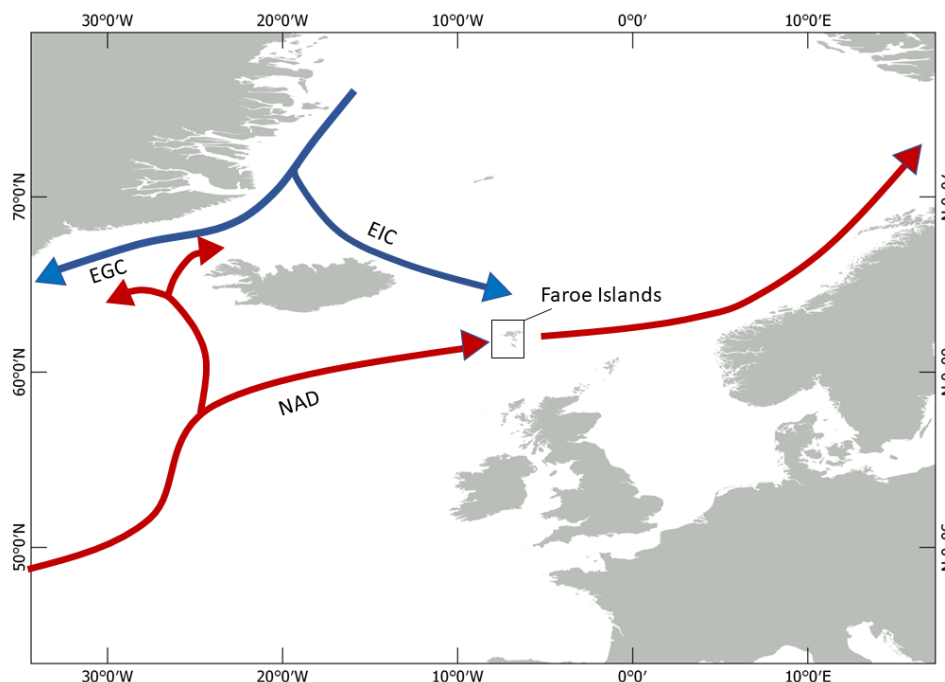


Figure 1. The location of the Faroe Islands in the North Atlantic Ocean and a schematic view of major oceanic surface currents. Red denotes a warm current while blue denotes a cold current.

2.2. Governing Climate Mechanisms

The climate variability of the North Atlantic Ocean is the product of several interconnected mechanisms, with major drivers being the AMOC and NAO. Given the maritime setting of the Faroe Islands, these large-scale climate patterns govern Faroese climate variability. The AMOC describes the collective flow of oceanic currents in the North Atlantic, driven by atmospheric and thermohaline pressure gradients. This produces a net poleward transport of heat and subsequent equatorward transport of cold deep water, in turn ameliorating high latitude climates and decreasing the latitudinal heat gradient. The AMOC varies in strength according to the amount of water and heat transported, partly governed by the North Atlantic deep-water (NADW) formation (Buckley and Marshall, 2016). A strong AMOC entails a stable transport of warm waters to high latitudes, while a weak AMOC decreases the oceanic poleward heat transport (Marshall et al., 2001). The NAO describes atmospheric zonal pressure gradient variations over the North Atlantic on interannual to multidecadal timescales (Hurrell, 1995). The strength of the pressure gradient between the Azores high and Icelandic low determines the phase of the NAO, being either positive (steep gradient) or negative (weak gradient) (Hurrell and Deser, 2010; Hurrell, 1995). The shifting phases of the NAO are associated with the strength of westerly winds, the position of storm tracks as well as temperature and precipitation variations over the wider North Atlantic area (e.g., Olssen et al., 2012).

One of the important controls on the climate of the Faroe Islands is their location in respect to oceanic currents (Andresen et al., 2007). The warm North Atlantic Drift (NAD), a continuation of the Gulf Stream, passes the islands on its route northward along the Norwegian coast. In an opposing southward direction off the eastern Icelandic coast, flows a branch of the cold East Greenland Current (EGC) called the East Icelandic Current (EIC). The Faroe Islands lie at the interface of these contrasting surface currents (Figure 1). These currents are key components of the AMOC, denoting its impact on the climate variability of the Faroe Islands. During periods when the NAD is weakened (weak AMOC), the EIC is further displaced towards the islands and cold polar waters extend southwards. Under such periods, arctic conditions probably prevailed at all elevations (Humlum and Christiansen, 1998). A stronger NAD (stronger AMOC) on the other hand implies that the Faroe Islands lie continually within its trajectory (Humlum and Christiansen, 1998). The position of the Faroes between these shifting current boundaries makes them interesting from a paleo-perspective, as they should register environmental responses to these shifts.

The Faroe Islands are located close to the North Atlantic cyclone tracks. The cyclones bring heavy precipitation, winds and increased heat to higher latitudes (Zhang et al., 2004). As such, their variability exerts a major control on the Faroese climate. Being frequent recipients of cyclones, combined with their exposed maritime location, explain the high wind speeds and heavy precipitation that characterise

the islands. Most cyclones arrive from the south or west, which is reflected in the dominating direction of incoming winds (Cappelen and Laursen, 1998; Christiansen and Mortensen, 2002). The most severe cyclones in the north-eastern Atlantic and consequently the Faroe Islands, develop during autumn and winter (Feser et al., 2015; Cappelen, 2020). This is mirrored in precipitation and windiness seasonality, both being more pronounced in the winter months (Cappelen, 2020; Cappelen and Laursen, 1998). Cyclone activity, together with many other climate expressions in the North Atlantic, are highly connected to the modes of the NAO (e.g., Feser et al., 2015). A positive phase is related to a northward shift of the storm track with increased transport of heat and precipitation bearing cyclones to higher latitudes (Hurrell and Van Loon, 1997; Feser et al., 2015). The opposite is true for a negative phase, where cyclonic systems instead shift to the Mediterranean area (Hurrell and Van Loon, 1997; Feser et al., 2015). Observed NAO records are relatively short and there exist but a few proxy records of Holocene NAO variability (e.g., Olsen et al., 2012; Faust et al., 2016; Nesje et al., 2000). The limited Holocene records of both the NAO and the Faroese paleoclimate suggest that millennial time scale NAO influences on Faroese environments remain somewhat uncertain.

2.3. Holocene Climate in the Faroe Islands

2.3.1. Early to Mid-Holocene Climate

The last glaciation to occur on the Faroe Islands ended during the Younger Dryas-Holocene transition (~12 100-11 700 yr BP), as indicated by basal dates of lake sediments (Olsen et al., 2010; Humlum and Christiansen, 1998; Andresen et al., 2006). This is further suggested by concurrent high offshore sedimentation rates on the Faroe shelf, possibly induced by meltwater discharge from the melting ice cap (Nielsen et al., 2007). Several paleoenvironmental studies covering the early Holocene have been conducted (Hannon et al., 2001, 2003, 2010; Andresen et al., 2007; Jessen et al., 2008; Björck et al., 2001). The newly deglaciated Faroese landscape was characterised by sparse fellfield tundra vegetation, with poor soil development and indications of heavy erosion (Jóhansen, 1985; Hannon et al., 2010; Lawson et al., 2008; Olsen et al., 2010). The vegetation gradually developed into an arctic heathland with *Betula nana*, *Salix herbacea*, *Juniperus*, *Empetrum* and *Ericaceae* by ca 10 250 cal yr BP (Hannon et al., 2003; 2010; Jóhansen et al., 1985). The vegetation succession along with rapidly increasing biogenic silica (Andresen et al., 2006) and aquatic pollen contents (Hannon et al., 2003), in lacustrine sediment from two sites, indicate a climatic warming and developing soils. The climate was however highly dynamic with several rapid shifts and cooling events inferred from proxy data, often attributed to meltwater outbursts and subsequent weakening of the AMOC (Jessen et al., 2008; Björck et al., 2001; Olsen et al., 2010; Hannon et al., 2003).

A transition from drier and seasonal subarctic climate to moister oceanic conditions before ~10 250 cal yr BP is inferred from a decline of *Betula nana* and a subsequent dominance of grasses and sedges (Hannon et al., 2003; 2010; Jóhansen, 1985). Towards the mid-Holocene a woody shrub-dominated vegetation is developed, indicating warmer temperatures (Jóhansen, 1985; Hannon et al., 2001). A mild climate with increased vegetation cover, organic productivity and a strong northward oceanic heat transport are further suggested by several proxy studies (Olsen et al., 2010; Andresen et al., 2006; Curtin et al., 2019). These studies infer a Faroese Holocene Thermal Maximum around 9000 to 7500 cal yr BP, roughly aligning with a nearby sea surface temperature reconstruction indicating maximum Holocene temperatures from 10 300 to 8 300 cal yr BP (Rasmussen and Thomsen, 2010).

Starting in 8000-7000 cal year BP a cooling trend that further intensified at c. 4000 cal yr BP commenced, as indicated by a wide array of proxies (e.g., Jóhansen, 1985; Olsen et al., 2010; Rasmussen and Thomsen, 2010; Andresen et al., 2006; Curtin et al., 2019; Marcott et al., 2013). This climate deterioration has continued into modern times and is synchronous with indications from plant wax isotopes that the Faroe Islands became progressively drier throughout the Holocene (Curtin et al., 2019). The cooling and decreasing moisture availability has been attributed to weakened northward heat and moist transport (Curtin et al., 2019) and reduced NADW formation (Olsen et al., 2010), suggesting that a slowdown in the AMOC is the main driving process on millennial timescales.

2.3.2. Human Colonisation

The timing of human colonisation on the Faroe Islands have traditionally been linked to the Norse expansion around 1150 cal yr BP (800 CE), from where direct archaeological evidence is found (Arge et al., 2005; Vickers et al., 2005; Church et al., 2005). A growing number of studies suggest an earlier period of settlement instead, as early as ca 1450 to 1250 cal yr BP (500-700 CE), inferred from pollen assemblages (Hannon et al., 2001; 2005; Edwards et al., 2005; Hannon and Bradshaw, 2000), carbonised barley grains (Church et al., 2013) and ancient DNA and faecal biomarkers (Curtin et al., 2021). These studies could corroborate a near-contemporary historical source describing Irish monks settling remote North Atlantic islands (Tierney, 1967). Human arrival was earlier suggested to bring with it the disappearance of woody shrubs and the onset of the current grass heath dominated vegetation, mainly through animal husbandry (mostly sheep) and grazing (Hannon et al., 2001; Jóhansen, 1985; Hannon and Bradshaw, 2000). Some studies have implied, however, that this transition occurred prior to human settlement (Hannon et al., 2005; Curtin et al., 2019). The grazing of sheep could therefore have exacerbated naturally occurring processes. Any anthropogenically driven environmental change would hence be superimposed on climatically driven ones (Hannon et al., 2005). Expansive woodland vegetation was not present on the Faroe Islands when humans arrived, which means that no widespread deforestation could occur. Lawson et al. (2005; 2008) showed that anthropogenic impacts on a local

landscape was relatively minor, with the current landscape resembling the pre-settlement one. This implication, along with the late arrival of humans, allows for a relatively unique opportunity to study Holocene environments where anthropogenic influence has been minimal.

2.3.3. Tephra Deposition

The Faroe Islands' proximity to Iceland makes them frequent recipients of volcanically derived tephra. Throughout the course of the Holocene, several tephra deposition events have been identified in Faroese lakes and mires (Wastegård et al., 2018). Some of the most widely dispersed tephra deposits on the Faroe Islands include the Saksunarvatn (~10200 cal yr BP), Mjáuvötn (~6600 cal yr BP), Hekla 4 (~4300 cal yr BP), Hekla Selsund/Kebister (Hekla S, ~3700 cal yr BP) and Landnám (1073 ± 2 cal yr BP) tephtras (Wastegård et al., 2018). Tephtras with andesitic, dacitic and rhyolitic compositions, e.g. Hekla 4 and Hekla S, are widely dispersed in both peat and lake sediment on the Faroe Islands (Wastegård et al., 2018). Basaltic tephtras on the other hand, e.g., Mjáuvötn and Landnám, are seldomly recorded in peat, implying poor retention of basaltic tephtra in these environments (Wastegård and Davies, 2009; Wastegård et al., 2018). Deposited tephtra is commonly remobilized on the Faroe Islands (Wastegård et al., 2018), reflecting their susceptibility to storm events and strong winds being able to rework previously deposited material.

2.4. Mire Development

2.4.1. Peat Accumulation and Mire Development

Peat formation occurs where long-term net primary production exceeds organic matter decomposition, allowing partially degraded organic matter to accumulate (Wieder et al., 2006). Peat accumulation is promoted in waterlogged soils where anoxic conditions prevail, inhibiting microbial respiration and decomposition of organic material. The balance between peat accumulation and decomposition is largely determined by the hydrological conditions in the actrotelm, the upper aerated section of a peat profile where decomposition can occur (Chambers et al., 2012). Temperature also exerts control on peat accumulation partly through controlling evapotranspiration, with cooler conditions inhibiting decomposition (Vitt, 2006). In other words, peat accumulation is promoted in areas characterised by wet and cool conditions. This is reflected in that areas with extensive peat, called mires or peatlands, are most common in cool and moist regions at mid- and higher latitudes (Tarnocai and Stolbovoy, 2006; Wieder et al, 2006).

Mires mainly form either through the process of paludification, in wet conditions over poorly drained mineral soils, or by terrestrialization, where litter gradually fills in shallow bodies of water (Kuhry and

Turunen, 2006). In this early stage the mire is often connected to ground and surface waters, which means nutrients are primarily supplied from surroundings mineral soils and bedrock (minerotrophic). Such mires are called fens and characterised by a relatively large nutrient input and alkaline to slightly acidic conditions (Vitt, 2006). Continued peat accumulation and vertical growth could cut off the fen surface from its ground or surface water supply, whereby water and nutrients are solely derived from atmospheric deposition (ombotrophic). The fen has now transitioned into a bog, with poor nutrient input and prevailing acidic conditions (Kuhry and Turunen, 2006). The fen to bog transition also often entails the initiation of *Sphagnum* dominance, whose decay resistant and acidifying litter intensify peat accumulation and vertical growth (Rydin et al., 2006). Areas with high precipitation and low evapotranspiration, conditions often found at high latitude maritime sites, may develop blanket mires where peat covers much of the landscape (Gorham, 1957).

2.4.2. Peat in the Faroe Islands

The Faroe Islands are wet and cold, which forms ideal conditions for peat to accumulate. Peat is consequently a widely distributed feature of the Faroese landscape with mires not only covering valleys and basins but also high elevation slopes (blanket mire), where they gradually transition into more minerogenic 'peaty' soils (Rasmussen, 1982; Jóhansen, 1985; Humlum and Christiansen 1998). *Sphagnum*, while widely present (e.g., Lawson et al., 2007; Persson, 1968), seldom dominates the mire vegetation which instead mainly consist of *Eriophorum angustifolium* and several *Carex* species (Hansen and Jóhansen, 1982; Hannon et al., 2001). Peat started to accumulate in the Faroe Islands around 9000 cal yr BP but various initiation dates are evenly spread throughout time, with a possible intensification between ca 6000 and 4000 cal yr BP (Lawson, 2007). The peat formation and expansion are attributed to local topographical, hydrological and pedological responses to long-term climate, rather than single climatic events or anthropogenic impacts (Lawson et al., 2007).

The current Faroese peat horizon is generally thin, seldomly extending 3 m depth and averaging 1-1.5 m (Rasmussen, 1982). Previous peat paleostudies have shown that peat accumulation rates have varied regionally and locally on the Faroe Islands (Lawson et al., 2007). For example, Shotyk et al. (2005a; b) retrieved a 72-cm long sequence that had accumulated for ~6300 years (Mýrararnar), while Lawson et al. (2007) found a 120-cm long sequence accumulating for ~5700 years (Sandoy) and lastly Wastegård (2002) reported that a 171-cm sequence accumulated over ~9000 years (Suduroy). These values can be contrasted against peat sequences of southern Sweden where 568 cm of peat accumulated during ~8500 years and 390 cm during ~8300 years (Kylander et al., 2013; Sjöström et al., 2020) and Islay, Scotland where a peat core of 391 cm accumulated for 6670 years (Kylander et al., 2020). The accumulation rate of peat and consequently the temporal resolution of Faroese mires is hence comparably low, which is reflected in the generally thin peat horizons. Possible explanations for the thin peat cover include

historically low primary production and/or high peat decomposition. Another source of reduced peat cover is peat cutting which has been widespread during the relatively short presence of humans on the Faroe Islands, being an important source of fuel in a treeless environment (Lawson 2005; 2007; Church et al., 2005). The peat was generally extracted in sequences from the top down (Persson, 1968), which means that disturbed peat profiles could be missing their uppermost section.

2.5. Geochemical and Physical Proxies in Peat Environmental Reconstructions

2.5.1. Peat as an Environmental Archive

Because mires are affected by climatic parameters (temperature and precipitation), sequester nutrients (atmospherically, hydrologically or autochthonously derived) and grow vertically in a chronological sequence from older (bottom) to younger (surface), any change in peat composition or characteristics could give indications on past climates, growing conditions and nutrient supply. As such, mires are valuable archives of environmental change (Chambers et al., 2012; Chambers and Charman, 2004; Bindler, 2006; Blackford, 2000). Historically, many paleoenvironmental studies on peat have focused on visual stratigraphy (e.g. Blytt, 1876; Sernander, 1908) and biological proxies such as pollen and macrofossils (e.g. Barber et al., 2003; Birks, 1981; Woillard, 1978). Geochemical techniques have perhaps been most prominent in tracing atmospheric heavy metal deposition history (e.g. Martínez Cortizas et al., 1997; 1999; 2002; Shotyk et al., 1997; 2001; Weiss et al., 1999; Kylander et al., 2005; Renberg et al., 1994; Bindler et al., 2004). An increasing number of studies employ geochemical techniques to relate to climatic processes through, e.g., relating Hg accumulation to paleotemperatures (Martínez Cortizas, 1999), identifying mineral paleodust source characteristics and changes (e.g. Kylander et al., 2007; 2013; Sjöström et al., 2020; Martínez Cortizas et al., 2020; Shotyk et al., 2002) and storminess reconstructions (Björck and Clemensen, 2004; De Jong et al., 2006; Orme et al., 2015; 2017; Stewart et al., 2017; Schofield et al., 2010; Kylander et al., 2020). Climatic information in the above-mentioned studies is inferred from a wide array of geochemical and geophysical proxies, including elemental concentrations and ratios, grain size changes, ash content, bulk density, decomposition and stable isotopes.

2.5.2. Methods in Peat Paleoenvironmental Reconstructions

2.5.2.1. Chronology and Peat Properties

Peats contain high amounts of carbon and plant macrofossils and are as such suitable for radiocarbon dating, a commonly deployed technique in obtaining peat chronology. The method builds upon the

radioactive decay of the unstable ^{14}C isotope, which is activated following the death of an organism. This gradually changes its ratio with the stable isotopes of carbon from the time of incorporation in an organism when it largely reflects the atmospheric ratio (for terrestrial plants). The ratio can be measured using Accelerator Mass Spectrometry (AMS), which together with the half-life of ^{14}C can be used to establish the age of dated samples. With the acquired ages, an age-depth model can be used to construct a chronology for the peat sequence (e.g. Blaauw and Christen, 2011). The atmospheric ratio has not been constant over time which yields discrepancies between ^{14}C years and calendar years. This can be corrected for using calibration curves (e.g. Reimer et al., 2020).

Bulk density variation in a peat sequence can be used for alignment of cores (e.g. Sjöström et al., 2020; 2022; Kylander et al., 2020) but has also been used as a proxy for peat decomposition when its organic fraction is considered (e.g. Björck and Clemmensen, 2004). This is based on the idea that more decomposed peat is more fine-grained and denser, yielding higher bulk density values. The degree of decomposition may be indicative of the hydrological conditions at the time of peat accumulation, where a highly decomposed peat infers oxygenated drier conditions with longer residence times in the acrotelm (Chambers et al., 2012). Other factors determining peat decomposition include the plant species composition (Yeloff and Mauquoy, 2006) and fertilisation by e.g., volcanic ash, sea spray (Broder et al., 2012) or dust deposition (Kylander et al. 2018, Sjöström et al. 2022, and Schillereff et al. 2021). The ash content of a peat represents the fraction retained after ignition (opposite to loss on ignition), which e.g. can provide important information on inorganic or mineral input variation to the peat (e.g. Kylander et al., 2020).

2.5.2.2. Elemental Geochemistry

Elemental geochemical composition of peat sequences can be obtained with XRF. This is a non-destructive analytical method which builds upon X-Ray irradiation of a sample and measurement of released radiation from excited atoms (fluorescence). The signature of the fluorescence can be attributed to a specific element which allows examination of elemental variation in a peat sequence. Several paleoenvironmental signals may be extracted from elemental data, including atmospheric dust fluxes from conservative lithogenic elements such as Si, Al, Ti, Zr, Ga, K and Y (e.g. Shotyk et al., 2001; 2005; Martínez Cortizas et al., 2020; Kylander et al., 2013; Sjöström et al., 2022; Chambers et al., 2012), redox conditions from Fe and Mn (Chesworth et al., 2006) and the often oceanically derived Br, Cl and Sr having been used as proxies for storms and oceanic input (Orme et al., 2015; Schofield et al., 2010; Stewart et al., 2017; Shotyk et al., 2002; Chambers et al., 2012) or decomposition (Biester et al., 2004; 2006; Martínéz Cortizas et al., 2007).

2.5.2.3. Mineral Composition

Three techniques to infer mineral composition are used in this study, namely ATR-FTIR, XRD and SEM-EDS. Infrared spectroscopy techniques e.g., given ATR-FTIR, are non-destructive and fast methods of providing valuable information on a molecular level. Based on the spectral response from emitted infrared radiation on molecular bonds and structure, information on both organic and inorganic components can be gained (e.g. Martínez Cortizas et al., 2021a; b). A notable area of use lies in the identification of peat minerals (Martínez Cortizas et al., 2021a). This is a novel approach of identifying minerals in basaltic settings. XRD and SEM are additional analyses from which mineral information may be inferred, the former by identifying crystalline mineral structures from the diffraction of X-Rays and the latter by revealing particle specific elemental composition (Sjöström et al., 2022). SEM has a further advantage in that particle morphology can be examined.

2.5.2.4. Principal Component Analysis (PCA)

Complex geochemical datasets can be reduced with PCA, which allows for extraction of statistical associations within a dataset. Variables included in a PCA are grouped into principal components (PC) according to their co-variability, expressed as factor loadings ranging from -1 (strong negative association) and 1 (strong positive association). By grouping variables together in a PC and plotting factor scores with depth, their governing mechanisms and change through time can be assessed (e.g. Muller et al., 2008).

3. Study Area

The study area is a mire complex referred to as Mýrarnar, situated on central Streymoy, the largest island in the Faroese archipelago (Figure 2). The mire is located in a bowl-shaped plateau at 360 m.a.s.l., with surrounding mountaintops reaching up to nearly 750 m.a.s.l.. The ocean and the closest town of Vestmanna is found roughly 4 km to the west. The oceanic nature of the site is reflected in strongly enriched concentrations of Cl, S, Br and Se, attributed to marine aerosol input (Shotyk et al., 2005a). A dammed reservoir is centrally situated in the plateau, about 350 northeast of the coring site. Several smaller streams and ponds cover the mire surface, including close to the coring site.

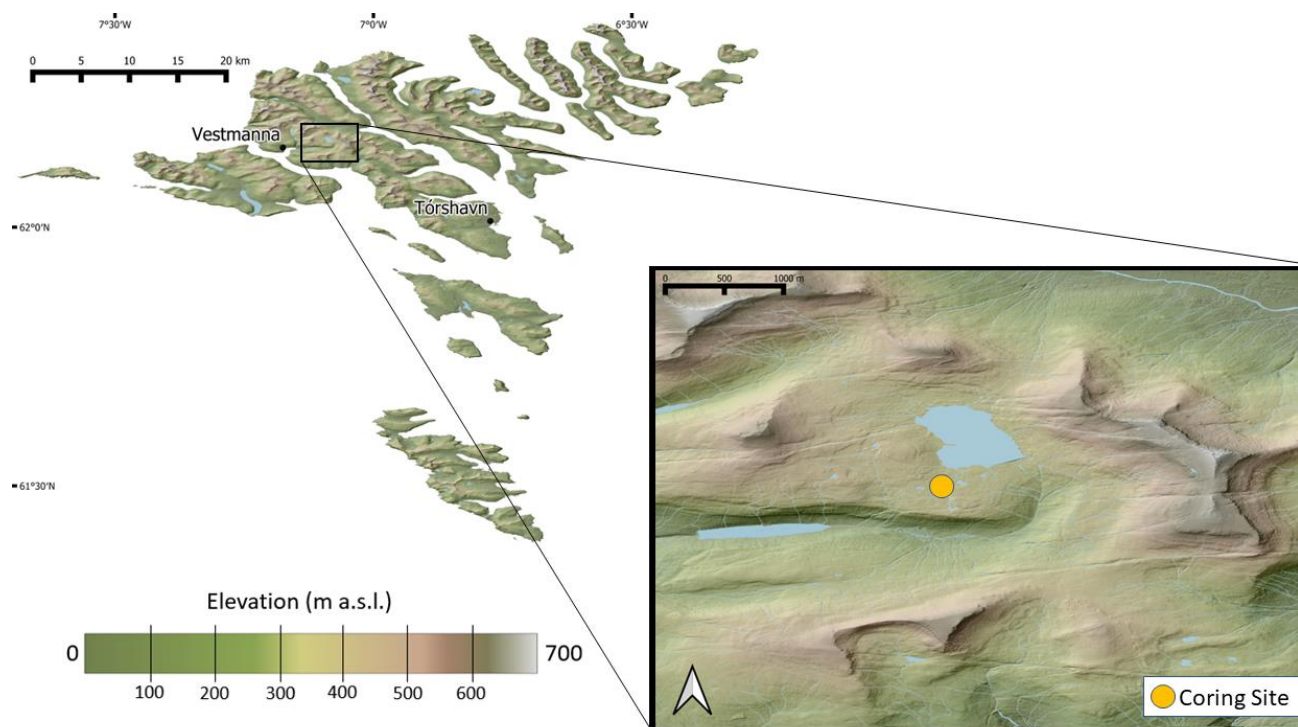


Figure 2. The location of Mýrarnar and the coring site on the Faroe Islands. With elevation data from the Polar Geospatial Center's ArcticDEM project (Porter et al., 2018).

Mean annual temperature and precipitation in Tórshavn (1981-2010), c. 23 km southeast of Mýrarnar, is 6.8 °C and 1321 mm respectively (Cappelen, 2020). As with the rest of the Faroe Islands, the climate is highly oceanic and precipitation is most concentrated in the winter months. Given the heterogeneity in the precipitation pattern, even on shorter distances, these values may not be representative of Mýrarnar. It may be assumed that precipitation is slightly higher here, owing to its location at a higher altitude and at the foot of larger mountains. The local bedrock and that of the Faroe Islands as a whole, consists of homogenous tertiary plateau basalts with a tholeiitic composition and phenocrysts of plagioclase (Rasmussen and Noe-Nygaard). The vegetation of Mýrarnar was described in detail by Persson (1968), where the mire surface was described as a moist grass heath with certain patches being

rich in *Sphagnum* species, including wetter parts dominated by *Eriophorum angustifolium*. The sample site of this study was in such an area, with surrounding vegetation noted to be rich in *Sphagnum* and sedges. Shotyk et al. (2005a) found that for much of their sequence, it took roughly 70 years to accumulate 1 cm of peat (or 0.014 cm/yr). This is roughly a fifth from rates found in northwestern Scotland and the nearby Shetland Islands (Shotyk, 1997). They further concluded, based on Ca/Ti and Ca/Sr ratios, that ombrotrophic conditions only prevail in the uppermost 58 cm of their core (5834 cal yr BP- to present) with conditions below this depth becoming increasingly minerotrophic.

4. Methods

4.1. Sampling

4.1.1. Field Sampling

The peat samples were collected in July 2021 from the south-western part of the wetland site of Mýrarnar at 62°09'41.0"N 7°05'29.0"W (Figure 2). A sequence of three cores were retrieved using a Russian Corer with a length of 1 metre and an inner diameter of 7.5 cm. The three sections were collected with an overlap of 25 cm from two adjacent boreholes to a bottom depth of 205 cm, with Core 1 (C1) corresponding to 0-100 cm, Core 2 (C2) to 75-175 cm and Core 3 (C3) to 105-205 cm. A primary stratigraphic description was made immediately following core retrieval, after which the cores were transferred to a pvc liner and wrapped in plastic film. The cores were later transported to and stored in a cold room (4 °C) at the Department of Geological Sciences at Stockholm University, where unless otherwise stated, all the following analyses/methods were performed.

4.1.2. Sub-sampling

The topmost surface of each core was removed using a stainless-steel knife. The cores were further cut into continuous 1-cm thick slices (n=300), from each of which a ~1x1-cm cube was cut to be used in bulk density calculations. Between each slice the knife was carefully cleaned to avoid contamination. The cube and remaining sample material of each centimetre were put into separate plastic zip-bags (the ones used for the cubes being pre-weighed) and subsequently placed in the freezer. After freezing, the cubes and the remaining samples were freeze dried at -59 °C in a Scanvac CoolSafe 55-4 Pro for three and four days respectively to remove all water.

4.2. Analyses

4.2.1. Radiocarbon Dating, Age-Depth Model and Growth Rate

Four depths were chosen for AMS radiocarbon dating, both attempting to achieve an even distribution throughout the profile and to capture interesting events as suggested by bulk density data. The chosen depths were 199-198 (D4), 133-132 (D3), 70-69 (D2) and 44-43 cm (D1). These samples were wet sieved in deionized water with the $>125\ \mu\text{m}$ fraction transferred to a petri dish, from which plant macrofossils (avoiding those being aquatic or having long-extending roots) were collected under a light-microscope. Most plant macrofossils picked out for dating were *Eriophorum* remains (Eleonor Ryberg, personal communication, Mauquoy and van Geel, 2007). The collected macrofossils were weighed, dried and sent for radiocarbon dating (see Table 1 for specifics). Macrofossils from D3 and D1 were sent to the Tandem Laboratory in Uppsala, Sweden, while D4 and D2 macrofossils were sent to Beta Analytic Inc. in Miami, Florida, USA. An age-depth model was constructed from the four dates, using the Bacon age-modelling software (v2.3.9.1) (Blauuw and Christen, 2011) with the IntCal20 ^{14}C calibration curve (Reimer et al., 2020) in R studios® (Appendix A for more information and settings). Growth rates (years per cm) were also obtained from the age-depth model.

4.2.2. Bulk Density, Core Alignment and Ash Content

The bulk density of each sample was estimated by dividing the dry weight of the cubes with their volume which was measured using a calliper. The bulk density was then used for core alignment, forming a composite core with a depth of 202 cm. Every other sample of the composite core ($n=102$) was dry ashed to determine the loss on ignition (LOI) and ash content (Dean, 1974; Sjöström et al., 2019). The crucibles were first dried to a constant weight at $105\ ^\circ\text{C}$ for 4 hours and subsequently weighed. The bulk peat samples were then added to the crucibles and again dried to a constant weight before being weighed (dry sample weight). Samples were then combusted at $550\ ^\circ\text{C}$ for 4 hours and weighed after cooling (ash weight). Ash content was estimated as percentage of ash (ash weight divided by dry sample weight). Growth rates (yr cm^{-1}) produced by the age-depth model together with bulk density (g cm^{-3}) was used to calculate the peat accumulation rates ($\text{g m}^{-2}\ \text{yr}^{-1}$) (PAR). Ash accumulation rates (AAR) for each depth was calculated as ash content multiplied by the PAR.

4.2.3. Elemental Geochemistry

4.2.3.1. X-Ray Fluorescence Core Scanner (XRF-CS)

Relative elemental concentrations for all cores were acquired using an ITRAX™ XRF core scanner. Before sub-sampling, XRF scans were performed on the fresh intact cores with scraped surfaces. XRF-

scanning for all cores was done using a molybdenum (Mo) tube with an exposure time of 40 s set at 30 kV and 50 mA with a step size of 5000 μm .

4.2.3.2. Wave-length Dispersive X-ray Fluorescence (WD-XRF)

Every third sample of the composite core was measured for absolute elemental concentrations through WD-XRF. The topmost samples were discarded due small sample sizes ($n=65$). Prior to analysis, roughly 600 mg of material was milled at 20 strokes per minute for 2 minutes with an ESSA Lab Wizz plant mill equipped with Teflon vials and agate milling balls. The samples were sent for analysis using a Bruker D8 VENTURE at the RIAIDT XRF facility of the University of Santiago de Compostela, Spain. Element concentrations received from WD-XRF analysis were multiplied with the PAR to get elemental mass accumulation rates (MAR).

4.2.6. Attenuated Total Reflection Fourier Transform Infrared (ATR-FTIR)

Spectroscopy

The ashed samples ($n=102$) were analysed with infrared spectroscopy using a Nicolet™ iS™ 5 Spectrometer equipped with an iD7 ATR device with a single reflection diamond crystal. The measurements were obtained for the spectral range 4000-400 cm^{-1} (2.5-25 μm) with a resolution of 4 cm^{-1} and the number of scans set to 100. Between each sample run, a new background was collected and the equipment was cleaned with ethanol.

4.2.7. X-Ray Diffraction (XRD) Mineral Analysis

Ashed peat samples from four depths of interest were selected for XRD analysis. Prior to analysis, the samples were transferred to plastic centrifuge tubes and treated with 15% HCl for 60 minutes. The tubes were subsequently filled with deionized water, put into an ultrasonic bath to disintegrate aggregates and centrifuged at 4000 rpm for 10. The deionized water is then decanted and replaced. This washing process was repeated three times. The samples were then treated with H_2O_2 for approximately 3 weeks. A 15% solution was initially used, with a 30% solution added after having reacted for around a week. To speed up the reaction, the centrifuge tubes were kept in a water bath where warm water was continually added. An extra sample was analysed for two depths, with one not having undergone any washing process at all and the other solely having been washed with HCl. This was done to assess potential impacts of various washing stages on sample composition. After washing all samples were finely milled using a mortar and pestle.

The analysis was done using a PANalytical X'Pert system equipped with X'celerator strip detector at the Department of Geosciences, Swedish Museum of Natural History. The samples were analyzed from 2° to $70^\circ 2\theta$, with a step size of 0.017° and a count time of 38 seconds. The instrument emits $\text{CuK}\alpha$

radiation ($\lambda = 1.5406 \text{ \AA}$) at 45 kV and 40 mA, passing through a curved graphite monochromator. Processing of the data was made in HighScore, a PANalytical software that allows mineral identification using integrated mineral reference patterns from the ICSD database (Bergerhoff et al, 1987).

4.2.8. Scanning Electron Microscope – Energy Dispersive Spectroscopy (SEM-EDS)

Analysis

Ashed peat samples from four of the depths analysed with XRD (including the unwashed and HCl-washed doubles, $n=6$) were further analysed with SEM-EDS at the Department of Geosciences, Swedish Museum of Natural History, using a FEI Quanta 650 field- emission scanning electron microscope. The instrument is equipped with an 80 mm² X-MaxN Oxford Instruments EDS detector (working distance 10 mm, beam size $>1 \mu\text{m}$, acceleration voltage 20 kV) allowing for elemental analysis and aiding mineral identification. Each sample was prepared in two separate ways. First, to examine particle morphology and surface chemistry, the samples were placed on an Al specimen stub. Secondly, to allow for chemical analysis of particle cross-sections, samples were placed in epoxy resin and polished with $3 \mu\text{m}$ and $1 \mu\text{m}$ diamond spray (Akasel) and subsequently coated with carbon. Reduction of spectra to chemical data, enabling calculation of approximate mineral formulas, was made within the AZtec software.

4.3. Statistical Analyses

Two separate PCA were conducted, one including ash and elemental data and one on the FTIR spectra, to explore statistical associations therein. The PCA on ash and elemental data was done on z-score transformed (to avoid scaling effects) AAR and MAR values respectively, following e.g. Sjöström et al. (2020) and Martínez Cortizas et al. (2019), with calculated MAR values ($n=65$) linearly interpolated to match the number of AAR values ($n=102$). The analysis was performed in JMP 15 software in correlation mode with a varimax orthogonal rotation. The number of components chosen to be extracted was based on the total explained variance, the Kaiser rule (eigenvalues > 1 , Kaiser, 1960) and scree test (Cattell, 1966). Reduction, statistical analysis and interpretation of FTIR data was performed by Prof. Antonio Martínez Cortizas. The raw data was standardised using z-scores. Peak identification and second derivative spectra were obtained in {andurinha}, a package for R (Álvarez Fernández and Martínez Cortizas, 2020). The PCA was done on a transposed spectra in the fingerprint region ($1800\text{-}411 \text{ cm}^{-1}$), as lower wavenumbers were deemed too noisy and the $4000\text{-}1800 \text{ cm}^{-1}$ region displayed no significant absorbance. Mineral reference spectra (Lafuente et al., 2015) allowed linking extracted components to specific minerals. Mineral phase variation throughout the sequence was inferred from plotting the PCA partial communalities (i.e., the fraction of the IR signal accounted for by each component) at every depth.

5. Results

5.1. Chronology

Calibrated ages (weighted mean) for the dated depths were 7793, 4267, 2473 and 1657 cal yr BP for D4, D3, D2 and D1 respectively (Table 1). The age-depth model calculated from these ages (Figure 3) give a basal age of 8005 cal yr BP (weighted mean). For the rest of the thesis, ages will be referred to as the nearest decade of the weighted mean calibrated ages produced by the age-depth model.

The age-depth model shows that the growth rate (yr cm^{-1}) has varied throughout the studied period. From 8005 to 4270 cal yr BP the growth rates are lower than in the remaining sequence with mean a mean $53.4 \pm 3.6 \text{ yr cm}^{-1}$ ($n=71$). From here it shifts to a mean of $29.1 \pm 2.2 \text{ yr cm}^{-1}$ until 1830 cal yr BP ($n=87$) from where the mean value is $40.1 \pm 2 \text{ yr cm}^{-1}$ towards the present ($n=45$). This gives a mean growth rate or temporal resolution of $40 \pm 11 \text{ yr cm}^{-1}$ throughout the sequence ($n=203$).

Table 1. Sample information and AMS radiocarbon measurements with calibrated age ranges and weighted means. Ua= Tandem Laboratory at Uppsala University, Beta= Beta Analytic Inc. The calibration was done using IntCal20 (Reimer et al., 2020) with 95% confidence intervals.

Name	ID	Top depth (cm)	Weight (mg)	Dated Material	^{14}C age (14C yr $\pm 1\sigma$)	Calibrated age range (cal yr BP. 2σ)	Calibrated weighted mean age (cal yr BP)
D1	Ua-73259	43	21	<i>Eriophorum</i> remains and <i>Carex</i> stems	1773 \pm 29	1553-1778	1657
D2	Beta-616095	69	19	<i>Eriophorum</i> remains and <i>Carex</i> stems	2420 \pm 30	2353-2693	2474
D3	Ua-73260	132	23	<i>Eriophorum</i> remains	3828 \pm 31	4103-4417	4267
D4	Beta-616096	198	7	<i>Eriophorum</i> remains, <i>Carex</i> stems and woody remains	6970 \pm 30	7675-7925	7793

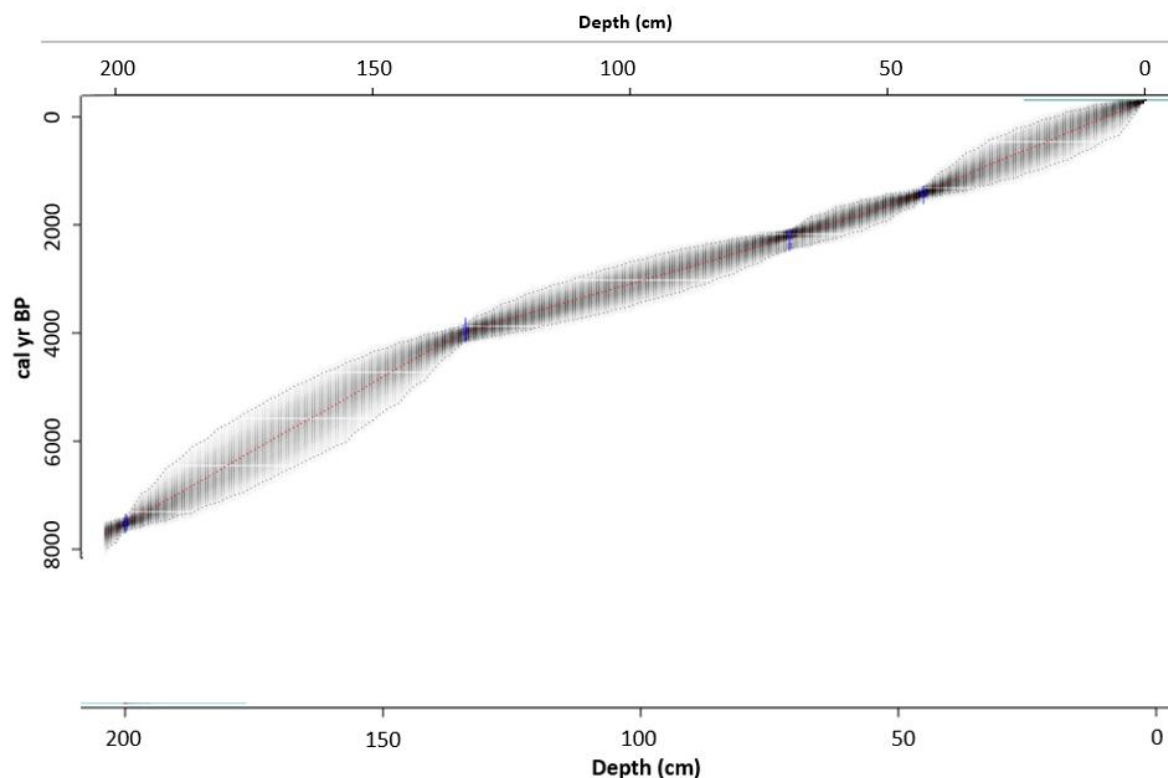


Figure 3. Age-depth model for the studied peat core constructed using 'bacon' in R. The grey shaded areas represent the 95% confidence range and the red dotted line represent the weighted mean of the calibrated ages.

5.2. Peat Properties

5.2.1. Visual Stratigraphy

Based on field observations, the oldest part of sequence until ~2330 cal yr BP is characterised by a visually homogeneous dark brown, fine grained and highly decomposed peat. Around 2330 cal yr BP until ~750 cal yr BP, distinct grass or sedge roots become prevalent. From ~620 cal yr BP towards the present the peat is dominated by *Sphagnum* mosses, with decreasing decomposition upwards. These interpretations were confirmed by the radiographic image produced by the core scanning. The sections ~6540-6000 and ~3460-2300 cal yr BP are noted to be less dense than the remaining sequence. Between ~4040 and ~3770 cal yr BP a rust-coloured precipitate coated the plastic liner beneath the core. Throughout the sequence, no clear tephra layers could be distinguished visually.

5.2.2. Bulk density, PAR, Ash Content and AAR

Bulk density ranges from 0.03 to 0.24 g cm⁻³, with an average value of 0.13 ± 0.03 g cm⁻³ (n=203, Figure 4). The maximum value is found at the bottom (8005 cal yr BP), with declining values to 0.15 g cm⁻³ at 7790 cal yr BP. Conversely, the lowest values are found at the top, with steeply decreasing

values from 0.13 g cm^{-3} at 620 cal yr BP towards the present. Outside these regions the bulk density variation is characterised by several peaks ranging from 0.17 to 0.18 g cm^{-3} , centred around 7740, 5790, 5360, 4100, 1920, 1250 and 1050 cal yr BP. There is also a baseline shift in bulk density around 4000 cal yr BP. The average bulk density from 7740 to 4020 cal yr BP is $0.15 \text{ g cm}^{-3} \pm 0.01$ ($n=74$), while the section between 4020 to 620 cal yr BP has an average value of $0.13 \text{ g} \pm 0.02 \text{ cm}^{-3}$ ($n=107$).

The PAR range from 5.8 to $63 \text{ g m}^{-2} \text{ yr}^{-1}$, with a mean value of $35 \pm 11 \text{ g m}^{-2} \text{ yr}^{-1}$ ($n=203$) (Figure 4). The PAR distribution displays the same peaks as those of the bulk density, including the shift around 4000 cal yr BP, but is heavily influenced by the nonlinear age-depth model. Consequently, the peat section between 7790 and 4490 cal yr BP display lower PAR (average $27 \pm 2.2 \text{ g m}^{-2} \text{ yr}^{-1}$, $n=75$) compared to the rest of the sequence up to 620 cal yr BP (average $43 \pm 7.5 \text{ g m}^{-2} \text{ yr}^{-1}$, $n=121$), reflecting the low growth rate of this section. The peak around 4130 is pronounced and represents the sequence maximum, after which values gradually decline towards the present, intercepted by the peaks at 1920, 1250 and 1050 cal yr BP.

The ash content ranges from 3 to 39% (average: $9.6 \pm 5.9 \%$, $n=102$), with the highest and lowest values found at the lowermost and most recent peat sections respectively. Much of the sequence have ash contents below 10% ($n=70$). From this baseline several peaks with ash contents from 10-35% occur ($n=$), largely aligning with those of the bulk density and PAR. An exception to this are the peaks at 1250 and 1050 cal yr BP in the bulk density and PAR profiles. Rather, a peak in ash content is centred around 820 cal yr BP. The AAR ranges from 0.18 to $22 \text{ mg m}^{-2} \text{ yr}^{-1}$ (average: $3.7 \pm 3.4 \text{ mg m}^{-2} \text{ yr}^{-1}$, $n=102$), with a distribution largely following that of the ash content (Figure 4). The peak at 4130 cal yr BP is however further pronounced and constitutes the sequence maximum.

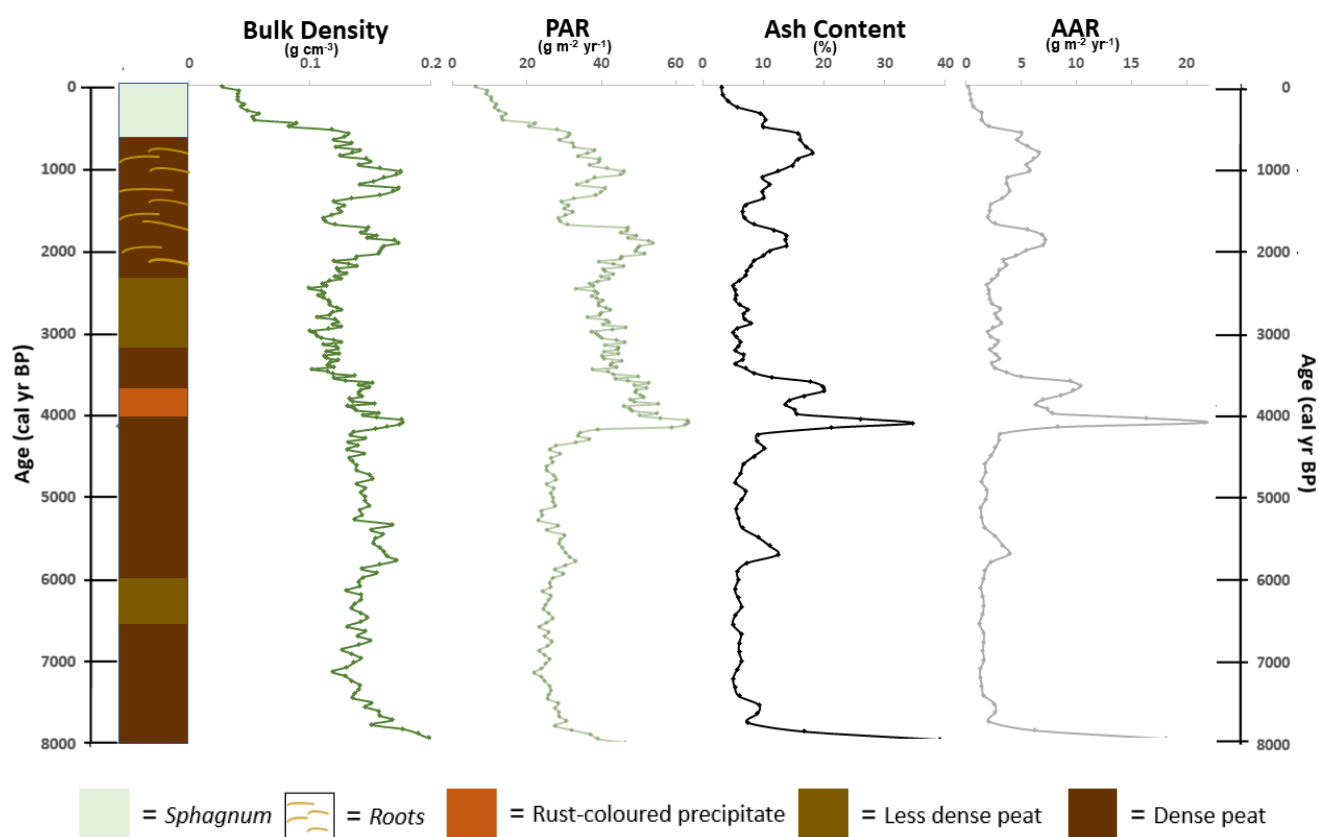


Figure 4. Visual stratigraphy, bulk density, peat accumulation rate (PAR), ash content and ash accumulation rate (AAR) plotted against age.

5.3. Elemental Geochemistry and PCA

The major elements throughout the sequence, measured by WD-XRF, are in decreasing order of average concentration: S ($4.2 \pm 1.7\%$), Fe ($2.5 \pm 1.3\%$), Si ($1.7 \pm 1.7\%$), Ca ($1.6 \pm 0.5\%$), Al ($1.0 \pm 0.5\%$), Ti ($0.7 \pm 0.6\%$), Cl ($0.2 \pm 0.1\%$), K ($0.08 \pm 0.09\%$), P ($0.08 \pm 0.07\%$), Mn ($0.04 \pm 0.02\%$) and Br ($0.03 \pm 0.001\%$) ($n=65$). Remaining elements (As, Cr, Ga, Nb, Ni, Se, Rb, Sr, Th, Y, Zn and Zr) all have concentrations with average concentrations below 60 ppm. Variables included in the PCA were chosen according to analytical precision and relevance for the study (AAR, Al, Br, Ca, Cl, Cu, Fe, Ga, K, Mn, Nb, Ni, P, Rb, S, Se, Si, Ti, Y, Zn and Zr). Elemental concentrations from WD-XRF and XRF core scanning peak areas are largely coherent and behave similarly when exploring them using PCA. This means that profiles from two different analytical methods display similar trends, increasing the confidence in them being actual trends. As such, focus is on the MAR calculated from WD-XRF absolute concentration data and PAR. XRF core scanning elemental peak areas along with all individual element concentration profiles can be found in the Appendix (A).

Four principal components (PC1-PC4) were extracted from the PCA and explain 86.4% of the total variance. PC1 accounts for 38.5% of the total variance and displays high factor loadings (>0.6) for Al, Ga, K, Mn, Nb, Si, Y, Zn and Zr together with the AAR, with moderately high loadings (0.3-0.6) for Cu, Fe, Rb, P and Ti (Table 2). PC2 accounts for 23.5% of the total variance with Br, Cl, Cu, Rb, Se, and Ti having high factor loadings and Al, Ga, K, Nb, Si and Sr having moderate ones. PC3 accounts for 15.3% of the total variance with Fe, Ni, S and Y having high factor loadings, with Cl (negative association), Mn and Nb having moderately high ones. Lastly, PC4 accounts for 9% of the total variance and display high factor loadings for Ca and P (negative association), with Mn having moderately high loadings. Several elements display associations with at least two components. Aluminum, Cu, Ga, K, Nb, Rb, Si and Ti all show at least a moderately high association both in PC1 and PC2. The same is true for Fe, Mn, Nb and Y between PC1 and PC3, Mn and P between PC1 and PC4, Cl and Nb between PC2 and PC3 and Mn and S between PC3 and PC4. Manganese and Nb are the only elements who display moderately high associations between three components.

Table 2. Variance explained by each principal component (PC) and factor loadings.

<i>Variable</i>	<i>PC1</i>	<i>PC2</i>	<i>PC3</i>	<i>PC4</i>
<i>% of variation</i>	38.5	23.5	15.3	9
<i>Cumulative %</i>	38.5	62	77.4	86.4
<i>Zr</i>	0.93	0.15	0.15	0.16
<i>Zn</i>	0.92	0.16	0.18	0.05
<i>Si</i>	0.89	0.33	0.05	-0.13
<i>K</i>	0.88	0.31	0.23	-0.12
<i>Nb</i>	0.86	0.33	0.32	0.10
<i>Al</i>	0.81	0.49	0.17	0.07
<i>AAR</i>	0.77	0.12	0.28	-0.11
<i>Ga</i>	0.76	0.53	0.11	0.19
<i>Sr</i>	0.75	0.50	0.00	-0.18
<i>Mn</i>	0.73	-0.15	0.31	0.53
<i>Y</i>	0.70	0.00	0.65	0.12
<i>P</i>	0.48	0.22	-0.20	-0.68
<i>Se</i>	0.02	0.91	0.08	0.15
<i>Br</i>	0.14	0.86	-0.01	-0.23
<i>Cu</i>	0.41	0.83	0.02	0.07
<i>Rb</i>	0.37	0.79	0.13	-0.24
<i>Ti</i>	0.36	0.75	0.08	-0.25
<i>Cl</i>	0.12	0.69	-0.36	-0.08
<i>Ni</i>	0.17	-0.05	0.91	0.09
<i>S</i>	0.14	0.13	0.90	0.34
<i>Fe</i>	0.49	-0.05	0.81	-0.02
<i>Ca</i>	0.26	-0.11	0.19	0.86

The variation of the PCs throughout the sequence can be depicted by plotting their factor scores against age (e.g. Muller et al., 2008) (Figure 4). The variability of PC1 show that elevated values or peaks are centred at 7790, 5740, 4130, 3680, 1960 and 820 cal yr BP (Figure 5). These peaks protrude from a seemingly flat baseline. The peak centred on 4130 cal y BP stands out from the rest in having distinctly high factor scores. PC2 scores display greater variability over time as compared to PC1. Initial values are high but drop to some of the lowest of the sequence between 7470 and 6050 cal yr BP. From here, a stepwise general increase can be inferred up to 1050 cal yr BP, after which values rapidly drop leading up to the youngest age (340 cal yr BP). Several peaks occur around 7790, 5740, 4350, 4020, 2020, 1290 and 1050 cal yr BP. The peaks at 7470, 2020 and 1050 cal yr BP have particularly high factor scores. Of further note for PC2 is a marked drop which is synchronous to the distinct peak at 4130 cal yr BP in PC1. PC3 shows relatively little variation throughout the sequence, except for one major peak between 3910 to 3690 cal yr BP. An anticorrelation with PC1 peaks (except at 3680 cal yr BP) can also be seen. This is most evident for the peaks at 7790 and 4130 cal yr BP. The final component, PC4, shows a stepwise decrease in factor scores until 4130 cal yr BP where elevated values are noted, followed by a decrease between 3910 and 3690 cal yr BP. This is anticorrelated to the main peak in PC3. After the drop, values increase to elevated levels by 3510 cal yr BP where they subsequently commence a fluctuating but generally decreasing trend towards the top of the sequence.

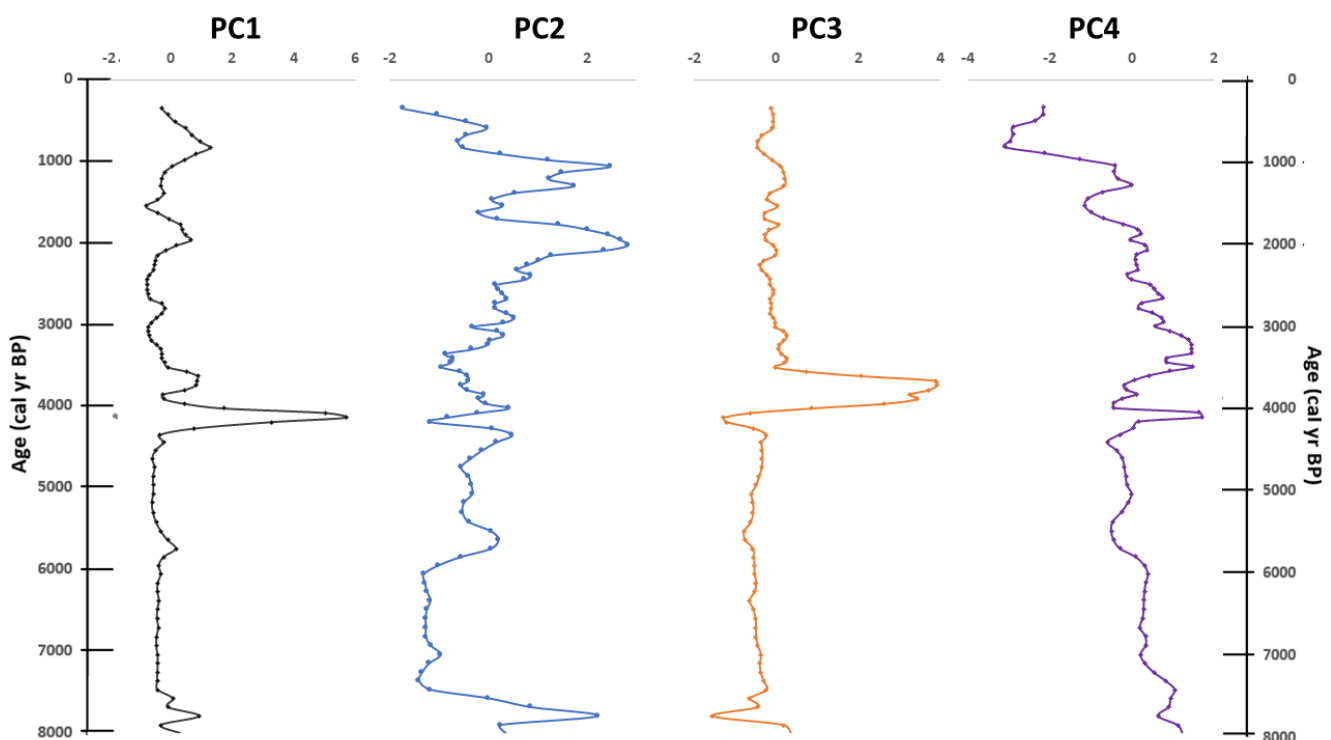


Figure 5. Factor scores plotted by age for each principal component (PC).

5.4. Mineral Composition

5.4.1. ATR-FTIR

Ten components were extracted from the PCA on FTIR spectra, with the last one accounting for less than 1% of the IR signal throughout the entire sequence. The first component is dominant and is interpreted to most likely represent minerals formed upon ashing and potentially organic matter. These show very high contents (average $80.8 \pm 11.3\%$ of the IR signal, $n=102$) for most of the sequence, with notable drops (down to 45.9% of the IR signal) centred around 7900, 5530, 4130, 3620, 1890 and 500 cal yr BP (Figure 5). The subsequent five components match reference mineral spectra well (Figure 5) and are therefore interpreted to represent plagioclase, quartz, anhydrite, calcite and anorthite respectively.

Plagioclase is the most common of these (average $7.3 \pm 5.4\%$ of IR signal, $n=102$) and is characterised by several peaks, with the highest contents found at 4130 cal yr BP (21.4% of the IR signal). The most notable plagioclase peaks all align with the drops found in the first component (minerals formed upon ashing and/or organic matter). For much of the sequence plagioclase contents might be relatively low (accounting for 1-5% of the IR signal), indicating a relatively low background input with elevated episodic supplies. Quartz (average $4.4 \pm 5.2\%$ of the IR signal, $n=102$) variation displays a similar pattern to that of plagioclase with several episodic periods of increased contents, the highest of which found at 7900 cal yr BP (23.4% of the IR signal), sharply increasing from periods of very low contents, or absence, of quartz. Peaks for quartz generally align with those of plagioclase, but with a more prominent peak found at 4440 cal yr BP. The peak at 4130 cal yr BP, having the highest plagioclase contents, is furthermore less pronounced for quartz (9.5% of the IR signal). Anhydrite contents (average $2.5 \pm 3.6\%$ of IR signal, $n=102$) are elevated by ~7640-5950 cal yr BP (up to 15.1% of the IR signal) and 3570-2800 cal yr BP (up to 10.6% of IR signal). For the rest of the record anhydrite content is generally very low (<1% of IR signal) with a few regions of slightly elevated contents (up to 3.1% of IR signal). Calcite contents are generally low (average $1.3 \pm 0.48\%$ of the IR signal, $n=102$), with the most elevated contents (2-2.1% of IR signal) found at 4960, 4640 and 4350 cal yr BP. Sharp decreases of calcite (down to 0.36% of IR signal) are noted at 7900, 7260, 6600, 5630, 4130, 3680, 2680 and 2200 cal yr BP. Many of these align with plagioclase and quartz peaks. Between 820 and 20 cal yr BP, there is a pronounced and prolonged drop to the lowest calcite contents of the sequence (down to nearly 0% of the IR signal). Anorthite contents are also generally low (average $1.2 \pm 0.9\%$ of the IR signal, $n=102$) and follow a similar pattern as that of calcite, sharing most of its peaks and drops in content.

The seventh component, although not clear, displays some similarities to the reference spectra of biotite or alternatively diopside (Figure 5). The potential biotite or diopside contents are overall very low

(average 0.3 ± 0.4 % of the IR signal, $n=102$), with notable peaks ($>0.5\%$ of the IR signal) protruding around 5840, 4640, 4130, 1890, 1380 and 340 cal yr BP. The highest contents are found at 4130 (up to 2.1% of the IR signal). The eighth component could not be tied to a reference mineral spectrum but shows some similarities to the Fe record (Appendix B) and is interpreted to represent Fe oxides. The contents are generally low (average $1.2 \pm 2.4\%$ of the IR signal, $n=102$) with peaks (1-4.3% of the IR signal) centred around 7900, 6710, 5630, 4640, 4130 and 3680 cal yr BP. After 1050 cal yr BP the values increase gradually to the sequence high at the present (11.2% of the IR signal). The remaining two components account for very low proportions of the IR signal throughout the sequence (averages $0.6 \pm 1\%$ and $0.1 \pm 0.1\%$ of the IR signal respectively, $n=102$) and could not be tied to a mineral phase, as such, they will not be further discussed.

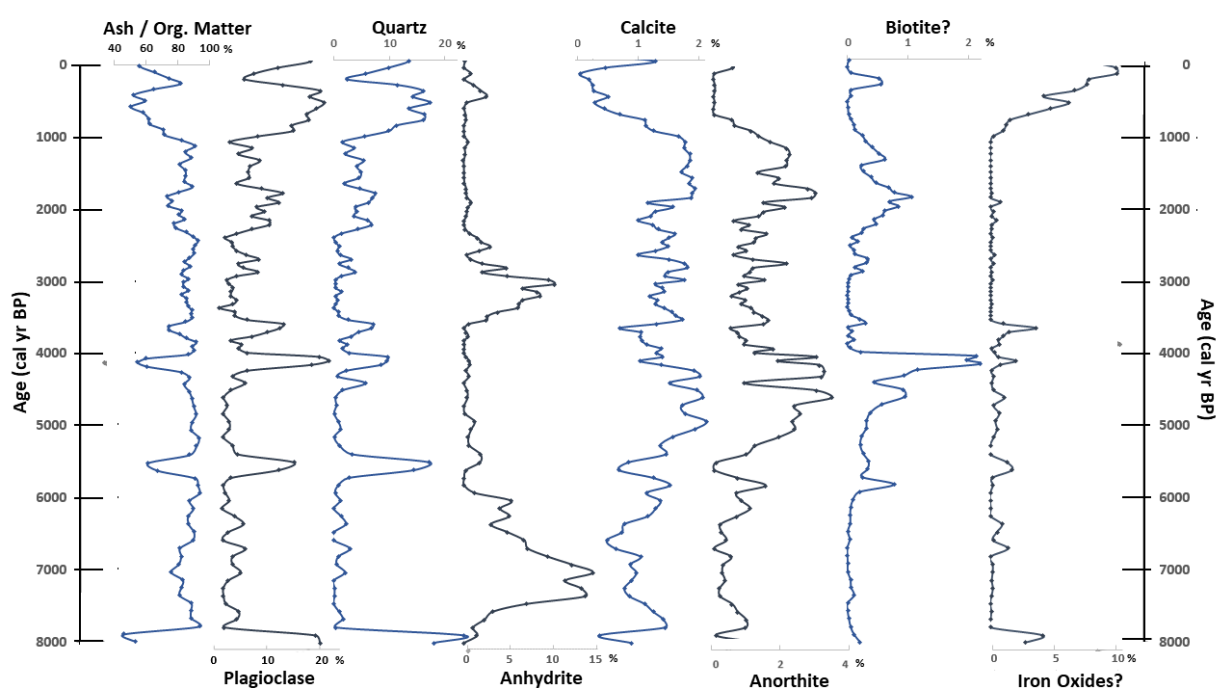


Figure 6. Fractionation of the communalities (squares of factor loadings) plotted by age for each component identified in the PCA for ATR-FTIR spectra.

5.4.2. XRD

Andesine, anorthite, quartz, coesite, diopside, hematite, bytownite and vaterite were identified in the XRD analysis from four depths (Table 3). Andesine is present in all samples and anorthite at 7000 and 820 cal yr BP, indicating the presence of plagioclases throughout the profile. Quartz is found at every depth except at 4130 cal yr BP and coesite is found at 4130 and 3740 cal yr BP. Hematite is only identified at 7740 cal yr BP while a minor fraction of magnetite is identified at 4130 cal yr BP. Bytownite is identified at 7000 cal yr BP and diopside and vaterite are identified at 800 cal yr BP, but only in samples not treated with H_2O_2 . A considerable amorphous component is inferred at 4130 and 3740 cal yr BP.

Table 3. Components identified with XRD analysis. Andes= andesine, An= anorthite, Qz= quartz, Coe= coesite, Di= diopside, Hem= hematite, Mag= magnetite, Byt= bytownite, Vtr= vaterite, Amorph= amorphous. X* denotes component only identified in samples not treated by H₂O₂. washi

Age (cal yr BP)	Andes	An	Qz	Coe	Di	Hem	Mag	Byt	Vtr	Amorph
820	X	X	X		X*				X*	
3740	X		X	X		X				X
4130	X			X			X			X
7000	X	X	X					X*		

5.4.3. SEM-EDS

Observations and elemental analyses made in samples dating to 7000 (including a sample only washed with HCl), 4130, 3740 and 820 (including an unwashed sample) cal yr BP (n=6) showed presence of tephra glass, plagioclase, quartz, hematite, ilmenite, zeolite, diopside and biogenic silica (Table 4). Tephra glasses dominate at 4130 and 3740 cal yr BP but are also widespread at 820 cal yr BP. These particles are characterised by irregular shapes and smooth surfaces with noticeable bubbles and vesicles (Figure 7A). The most common elements in these particles are Si, Al, K, Fe, Na and Ca. Plagioclase (mostly interpreted to be andesine) are found in every sample (Figure C) albeit in relatively low numbers when contrasted to the tephra glass. Quartz, zeolite and ilmenite are at least present at 7000 and 820 cal yr BP. Both angular and readily rounded particles of quartz exist, the latter of which suggests aeolian origin (Pye, 1987). Biogenic silica is at least present at 3740 and 800 cal yr BP. Much of this occurs as diatoms, which are especially widespread at 3740 cal yr BP (Figure 7D). Furthermore, Fe oxides with a chemical composition consistent with hematite are widely present here (Figure 7B). The hematite occurs as spherical particles that are widely observed in the sample from 3740 cal yr BP. Diopside is present in the unwashed sample of 820 cal yr BP but was not found in the washed sample.

Table 4. Components identified with SEM-EDS analysis. Pl= plagioclase, Qz= quartz, Hem= hematite, Ilm= ilmenite, Zeo= zeolite, Di= diopside, BSi= biogenic silica. X* denotes components only identified in samples not treated by H₂O₂.

Age (cal yr BP)	Tephra Glass	Pl	Qz angular	Qz rounded	Hem	Ilm	Zeo	Di	BSi
820	X	X		X		X	X	X*	X
3740	X	X			X				X
4130	X	X							
7000			X	X		X	X		

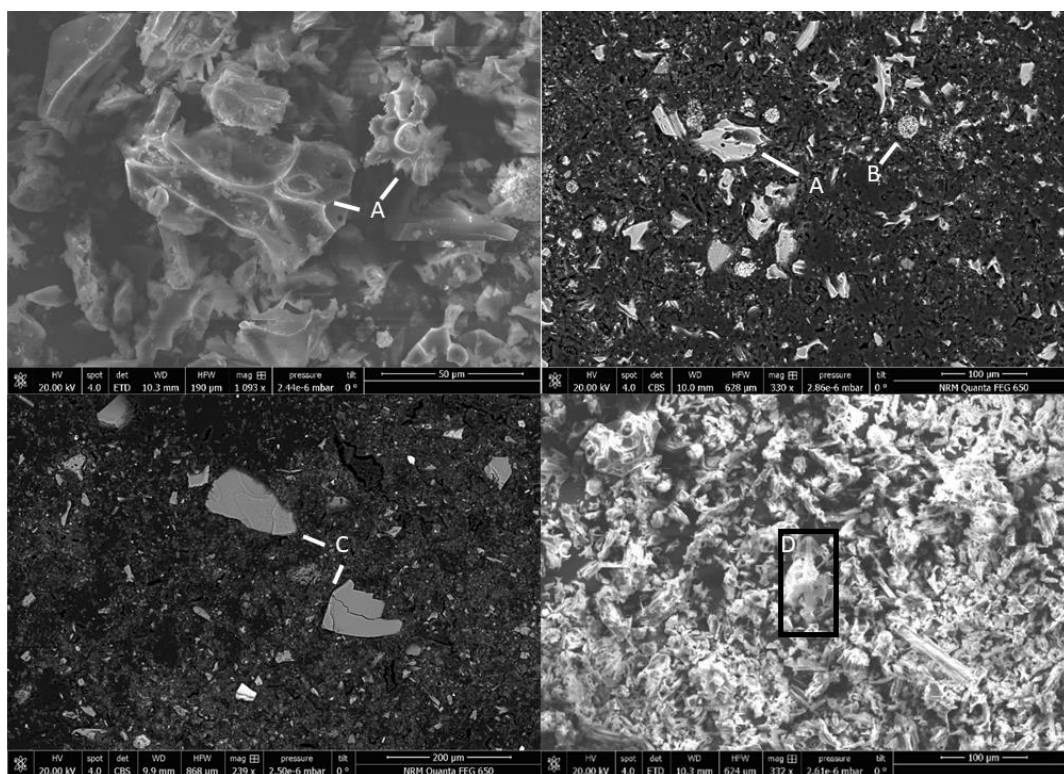


Figure 7. Images captured during SEM-EDS analysis. A= volcanic glass, B= spherical hematite, C= plagioclase, D= diatom.

6. Discussion

6.1. Deposit Characterisation

The lithology, age-depth model and the various data profiles of the studied peat sequence display no sign of any abrupt shifts or hiatuses. This suggests that peat has been continuously accumulating for ~8000 years. The bottom substrate could not be penetrated during coring and the bottommost part of the sequence has higher ash contents and bulk density. It is therefore most probable that the peat accumulated over dense minerogenic lacustrine sediments or saprolite. The sequence is characterised by a visually homogeneous dark, fine-grained and highly decomposed peat. Larger plant macrofossils are only visually distinguishable from ~2330 cal yr BP to the present, with grass or sedge roots being common up to ~620 cal yr BP after which *Sphagnum* is evident. The examined and dated depths of D4, D3, D2 and D1 (7793, 4267, 2474 and 1657 cal yr BP) are all dominated by sedges (*Eriophorum* and *Carex* spp), suggesting that growing conditions at Mýrarnar have been rather stable up until ~620 cal yr BP where *Sphagnum* becomes more dominant. However, the lack of full macrofossil analyses together with the highly decomposed nature of the material prevent identification of any vegetation

shifts on shorter timescales. The high peat decomposition could suggest that the primary production have been low and/or that the microbial respiration have been high. It is likely that the peat has been aerated, at least periodically, which would lead to more microbial activity and decomposition (Chambers et al., 2012). The mean growth rate found by Shotyk et al. (2005a) in the same mire complex is more than two times lower (83 yr cm^{-1}) and their sequence differs in temporal coverage with peat starting to accumulate ~ 1800 years later ($\sim 6200 \text{ cal yr BP}$). The current vegetation at the coring site resembles what Persson (1968) described as being indicative of the wetter parts of the mire. Thus, the higher growth rate and earlier peat initiation found in this study are most probably accredited to wetter conditions prevailing at the coring site, which would inhibit decomposition relative to drier parts of the mire. This highlights a spatial heterogeneity of peat accumulation within the mire and corroborates Lawson et al. (2007) who reasoned that individual peat accumulation histories on the Faroe Islands relate to local conditions, rather than climate.

Measured bulk density and ash contents in this study are comparable to those of previous studies from Mýrarnar (Shotyk et al., 2005a) and fall within typical ranges for high latitude peats (Chambers et al., 2011). The bulk density is noticeably influenced by the ash content, with most periods of elevated values in the former coinciding with peaks in the latter. These ash content peaks protrude from a rather constant sequence baseline. This indicates that there is an episodic supply of incombustible inorganic material to the mire. Removal of these episodic inorganic peaks from the profile allows for the examination of the bulk density without this high ash supply. The bulk density sequence could hence be interpreted as a rough approximation of organic bulk density and hence as a proxy for the degree of decomposition, with higher values indicating more decomposed peat and lower indicating less decomposed peat (e.g. Björck and Clemmensen, 2004). In doing so, a shift from higher to lower bulk density values near D3 (4270 cal yr BP) can be observed. A similar shift near D3 is also seen in the PAR and AAR profiles (Figure 4). In this case, it can at least be partly attributed to the non-linear age-depth model (Figure 3). The growth rates before $\sim D3$ are the lowest in the sequence (average $53.4 \pm 3.6 \text{ yr cm}^{-1}$, $n=71$) whereafter they shift to some of the highest in the sequence (average $29.1 \pm 2.2 \text{ yr cm}^{-1}$, $n=87$). Consequently, all accumulation rate data (PAR, AAR and MAR, all derived from the growth rate) will be affected by this shift produced by the age-depth model. This could be argued to be a major uncertainty as the age-depth model is produced from only four ^{14}C dates, between which more complex accumulation rate variations might have occurred. However, this shift is present in the bulk density and several elemental concentration profiles (e.g. Br, Ca, Cl, P, S and Se, Appendix B), which are values unaffected by accumulation rate variation. It is therefore argued that the accumulation rate data at least partly represents real change, despite the limitations of a low-resolution age-depth model.

6.2. Relationship between Geochemical Tools

In this thesis elemental variability has been established using XRF core scanning and conventional XRF (WD-XRF). Mineralogy has been explored using ATR-FTIR, XRD and SEM-EDS. The different analyses are based on different principles and as such do not provide identical information. The two different XRF techniques, while not identical, yielded similar patterns with elemental peaks roughly aligning in time and depth but not always in magnitude. The quantitative conventional XRF data therefore validates the XRF core scanning data. Nonetheless, the focus here will be on the conventional XRF data which provides a wider range of elements and quantified absolute concentrations (vs relative changes only).

The mineralogy inferred from XRD, SEM-EDS and ATR-FTIR analyses display more discrepancies. This is perhaps partly caused by them involving some element of interpretation. Morphology and chemical composition from SEM-EDS and amorphous components in XRD both inferred the presence of volcanic glass in the samples. This could not however be clearly identified with ATR-FTIR. Zeolites and ilmenite were furthermore widely identified in SEM-EDS but not with XRD or ATR-FTIR. All three techniques agree on plagioclases and quartz being the dominant non-tephra components, although the exact mineral assignment varies slightly. Treatment with H₂O₂ was found to remove bytownite, vaterite and diopside in the XRD analysis, which for diopside also was suggested by SEM-EDS. It is important to note here that in the SEM-EDS analysis only individual particles were examined and not every particle in a sample, which means that several components might be missed. This can be compared to the ~10 mg sample sizes used in XRD and ATR-FTIR analyses. Moreover, the approach of using ATR-FTIR for mineral identification in a basaltic setting is novel which means that further developments can be made. The discrepancies highlight that care needs to be taken in interpreting the results as different techniques may infer contrasting mineral compositions. Using the techniques in conjunction is however argued to be favourable in attaining a more accurate interpretation of the results.

6.3. Proxy Interpretation

6.3.1. Elemental Data

PC1 captures the variability of the AAR along with Al, Ga, K, Mn, Nb, Si, Sr, Y, Zn and Zr (strong loadings), elements often characterised as lithogenic (e.g. Kylander et al., 2013; 2021; Martínez Cortizas et al., 2020; Sjöström et al., 2020). Many of these elements can indeed be hosted in common minerals in the Faroese bedrock, including plagioclases, quartz, olivine, pyroxenes (augite and pigeonite) and zeolites (Rasmussen and Noe-Nygaard, 1970) and minerals identified in the XRD and SEM-EDS analyses (Table 3 and 4). The PC1 peaks are found at discrete depths and generally align

with peaks in bulk density and ash content. It may hence be deduced that peaks in bulk density and ash content (followingly also in PAR and AAR) are signals from episodic input of the lithogenic PC1 elements. The peaks are furthermore synchronous with inputs of plagioclase and quartz and to a lesser extent, the potential Fe oxides, as inferred from ATR-FTIR data (see below). This would imply that PC1 represents variation in mineral deposition.

The results from SEM-EDS analysis (morphology and chemistry) show that the prominent PC1 peaks at 4130, 3740 and 820 cal yr BP are dominated by tephra glass (Table 4 and fig 8). This is also supported by dominance of an amorphous phase in the XRD results at 4130 and 3740 cal yr BP (presence of large, and wide hump in the diffractograms, Appendix C) (Sjöström et al. 2019). These probably reflect all the tephra layers previously identified at Mýrarnar by Persson (1968), dated to 3650 ± 656 ^{14}C yr BP (~4120 cal yr BP), 3420 ± 105 ^{14}C yr BP (~3820 cal yr BP) and 900 ± 120 ^{14}C yr BP (~830 cal yr BP). In comparing these to previously identified Faroese tephra horizons, the first two can be attributed to the Hekla 4 (~4300 cal yr BP) and Hekla S (~3700 cal yr BP) tephtras respectively, with the latter likely being related to the Hekla 1 or Hekla 1158 tephtras (~850 and ~790 cal yr BP) (Wastegård et al., 2018). Hence, at least three of the PC1 events seem to represent tephra deposition following Icelandic volcanic eruptions. Shotyk et al. (2005a) interpreted peaks in Al, Ga, Mn, Si, Sr, Y and Zr (all associated with PC1 in this study) to represent volcanic deposition events at Mýrarnar. Other than for Hekla 4, Hekla S and Hekla 1/1158 however, the PC1 peaks cannot be related to the tephra layers found by Persson (1968) and do not align well with identified Faroese tephra horizons (Wastegård et al., 2018). Given this, it is not possible to confirm or reject the interpretation that PC1 solely represents tephra deposition. Thus, PC1 is interpreted to represent mineral deposition events, a term within which tephra deposition is included. At least 8 mineral deposition events are identified in the sequence, numbered 1-8 in chronological order (Fig x).

PC2 have strong loadings of the halogens Br and Cl, the typically lithogenic Rb and Ti as well as Cu and Se, which have high affinities for organic matter (McLaren and Crawford, 1973; Sharma et al., 1983). Bromine and Cl has previously been used as proxies of sea spray (Orme et al., 2015; Schofield et al., 2010; Stewart et al., 2017) but this has been questioned (Kylander et al. 2020). While Cl have been considered conservative in peats (Shotyk, 1997) and atmospheric Br has been found to be retained in peat humic acids (Zaccone et al., 2008), their post-depositional retention is complex and not only governed by atmospheric inputs (Biester et al., 2006). The most important mechanism of halogen retention in peat is the formation of organohalogens (Biester et al., 2004), formed by enzymatic halogenation by microbes (e.g. Shaw and Hager, 1959; Gribble, 2003). Most halogens in peat are found in organically bound forms and their concentration have been found to be heavily dependent on decomposition processes, with high halogen concentrations being correlated to high peat decomposition (Biester et al., 2004; Martínez Cortizas et al., 2007; 2016). This suggests that even though they are

oceanically sourced (and surely in excess), their presence at Mýrarnar is not only governed by oceanic input. Besides Br and Cl, also Se have been suggested to be affected by peat decomposition (Martínez Cortizas et al., 2007; Biester et al., 2006) and Cu has a high affinity to bind to decomposed organic matter (McLaren and Crawford, 1973). The implication here is that the PC2 elements do not mirror changes in atmospheric deposition, but rather changes in the organic fraction and decomposition of peat.

The association of the normally lithogenic Ti and Rb in PC2 could be explained by increased dust deposition during periods of high peat decomposition (favoured by drier climates). Titanium, however, is strongly associated with PC1 if the peat sections representing Hekla 4 and Hekla S are not included in the PCA. These tephras are relatively devoid of Ti when compared to others (Wastegård et al., 2002; Meara et al., 2020; Harning et al., 2018). Titanium is thus more strongly associated to the other lithogenic elements of PC1 throughout much of the sequence, but due to its relatively low abundance in the tephra layers, it is relocated to PC2 (which have no peaks for Hekla 4 and Hekla S). Rubidium on the other hand remains strongly associated with PC2 regardless of the tephra layers. The individual concentration profiles of Rb, Br and Cl closely resemble each other (Appendix B), indicating that similar mechanisms determine their presence in the peat. It is therefore suggested that the dominant form of Rb in the profile is organically bound and governed by decompositional processes.

It has earlier been shown that the deposition of volcanic ash (Broder et al., 2012) and mineral dust (Schilleref et al., 2021; Kylander et al., 2018; Sjöström et al., 2022) can have a fertilizing effect that promotes peat decomposition. The peaks of PC2 are mostly synchronous with the peaks of PC1, where most are in phase while some are anti-correlated. It is therefore speculated here that the PC2 peaks represent a response to the PC1 mineral deposition events, through fertilization that promotes peat decomposition and retention of the elements in PC2. Anti-correlated peaks, most prominently seen at Hekla 4 and Hekla 1/1158, are potentially caused by a dilution of the organic components caused by the high PC1 lithogenic input. Shared peaks could hence indicate more modest mineral deposition events while anti-correlated ones could represent greater lithogenic inputs. Alternatively, the events at shared peaks could denote deposition during drier climatic conditions where decomposition is promoted. With Hekla 4, Hekla S and Hekla 1/1158 (neither correlated or anticorrelated with PC2) being the only described tephra layers at Mýrarnar (Persson, 1968), it is likely that these will represent the most considerable lithogenic element inputs to the peat if other peaks also represent tephra deposition. This would explain the observed pattern. There is also a possibility that Hekla 4, Hekla S and Hekla 1/1158 are the only tephra horizons in the sequence, whereby the other peaks could represent mineral deposition events of another character and another impact on peat decomposition. Regardless of the mode of fertilisation, PC2 is here interpreted to represent decomposition, with higher loadings

indicating higher decomposition. To validate this interpretation however, independent measurements of peat decomposition are required.

PC3, besides displaying dilution effects following mineral deposition events, mainly captures a single event. This event is characterised by highly elevated factor scores from ~4000 and ~3700 cal yr BP, indicating increased importance of Fe, Ni, S and Y after Hekla 4 and through Hekla S and confirmed by the rust-colored precipitate observed coating the plastic liner. Spherical particles of hematite (Figure 7b) were found at least near the end of the event at Hekla S (here ~3740 cal yr BP), confirmed by both XRD and SEM-EDS analyses. A minor fraction of magnetite is also found near the onset of the event (XRD analysis) at Hekla 4. The Fe oxide presence in ashed peat indicated from ATR-FTIR data is accordingly elevated at these depths, but not in between (Figure 6). The PC3 event could be derived from Fe oxides and other compounds present in the tephras, through leaching of Hekla S and/or upwards diffusion from Hekla 4. XRD and SEM-EDS analyses suggested a much higher presence of Fe oxides at Hekla S than in Hekla 4, a distinction not reflected in the geochemical composition of the tephras (e.g. Wastegård et al., 2001). It would hence seem more probable that the PC3 signal and hematite is sourced from the Hekla 4 tephra, via diffusion and subsequent oxidation at Hekla S, as described by Steinmann and Shotyk (1997). This would imply that the Hekla S deposition induced oxic conditions enabling the formation of Fe oxides. This point of view requires that the ATR-FTIR interpretation is correct however, with no elevated presence of Fe oxides between Hekla 4 and Hekla S. If not correct, it is possible that hematite is found throughout PC3 which would imply that oxic conditions were instead instigated by the Hekla 4 deposition. PC3 will here be interpreted to represent a post-Hekla 4 event (Figure 8), with an upward relocation of PC3 elements derived from the tephra and subsequent oxidation in an oxic environment.

PC4 captures the variation of Ca, Mn and P (negative association). Calcium has the highest factor loading and its cations are known to diffuse vertically in peat profiles following weathering of underlying sediment (Steinmann and Shotyk, 1997). This typically results in a Ca profile where high concentrations in the base gradually decrease towards the surface (McKenzie et al., 2002). A similar pattern is seen in this study, but after the deposition of Hekla 4 the trend is reset. It is therefore suggested that the Hekla 4 tephra provided a new source from which weathered cations can be released and vertically diffused. Manganese has a stronger association with the PC1 elements which implies that mineral deposition events are the major control on its variability in the sequence. It is however known to be soluble and mobile in reducing environments (Boyle, 2001) and could here display a similar post-depositional behaviour as that of Ca. Phosphorus is negatively associated with Ca and Mn and as such its concentration increases upwards in the sequence, interrupted and reset by the Hekla 4 deposition. A primarily atmospheric source of P can instead be inferred, with downward movement. The behaviour

of these elements implies that PC4 represents vertical transport of Ca, Mn and P, with the Hekla 4 tephra acting as a barrier and/or source in this process.

6.3.2. Spectral Data

The spectral data from ATR-FTIR is used as supporting information in this thesis and as such, only a few selected identified mineral profiles are discussed. Of the identified minerals from spectral data in the sequence, plagioclase and quartz are the two most important (Figure 6). They furthermore display very similar profiles ($r=0.93$), indicating that similar processes determine their presence in the peat. Although to a lesser extent, the component interpreted to be Fe oxides generally shares peaks with plagioclase and quartz. The governing process seems to be the PC1 mineral deposition events, which share most peaks with the minerals identified in the spectral data. Some of the highest inferred contents of plagioclase, quartz and Fe oxides are found at Hekla 4, Hekla S and Hekla 1/1158. The presence of plagioclase and quartz in these horizons were further confirmed by XRD and SEM-EDS analyses (although no quartz was found in Hekla 4 and Hekla S in SEM-EDS). It is hence implied that; i) tephra deposition events affect the climate or local environment so that dust deposition with plagioclase and quartz is promoted, ii) that these mineral components are deposited along with volcanic glass as part of the tephra or crystallised from it (Friedman and Long, 1984) or iii), that both are true. The deposition of tephra may have the potential to reduce vegetational cover (Zobel and Antos, 1997), which in turn may increase erosion and dust deposition (Shotyk et al., 2002). This presents a potential mechanism for increased plagioclase and quartz input to the peat following tephra deposition. While this effect is expected to follow tephra deposition rather than being simultaneous as suggested in the data, the low temporal resolution (one cm represents in average 40 years) of the sequence and homogenisation by vegetation and its subsequent decomposition prevents us from seeing this kind of detail.

That the minerals are deposited as part of the tephra remains a plausible explanation, with both plagioclases, quartz and Fe oxides being described as components of Hekla tephra layers in Iceland (Andrews et al., 2006; Sverrisdottir, 2007). A major source of mineral input to the peat is hence suggested to be tephra deposition, given the minerals' relative importance at known tephra horizon. The windy character of the Faroe Islands and the frequent cyclones would likely be able to remobilise and redistribute the tephra, mineral and glass particles alike. Whether the other PC1 lithogenic input events with peaks in these minerals also are connected to tephra deposition, or represent independent processes, remains unresolved here.

Even though minerals are present in conjunction with tephra layers in the sequence, SEM-EDS analysis still indicated that volcanic glass dominated. This poses the question on how volcanic glass is represented in spectral data. It is possible that the volcanic glass signal is part of the first component

interpreted to represent minerals formed upon ashing and possibly organic matter. This component is anti-correlated with peaks with the known tephra layers however, which is not expected if the volcanic glass (the dominant fraction of the tephra) is included here. It is therefore speculated that the volcanic glass signal overlaps with those of the minerals. A next step could be to separate the volcanic glass from the matrix and retain its spectral signal, to isolate it and further constrain the spectral data interpretation.

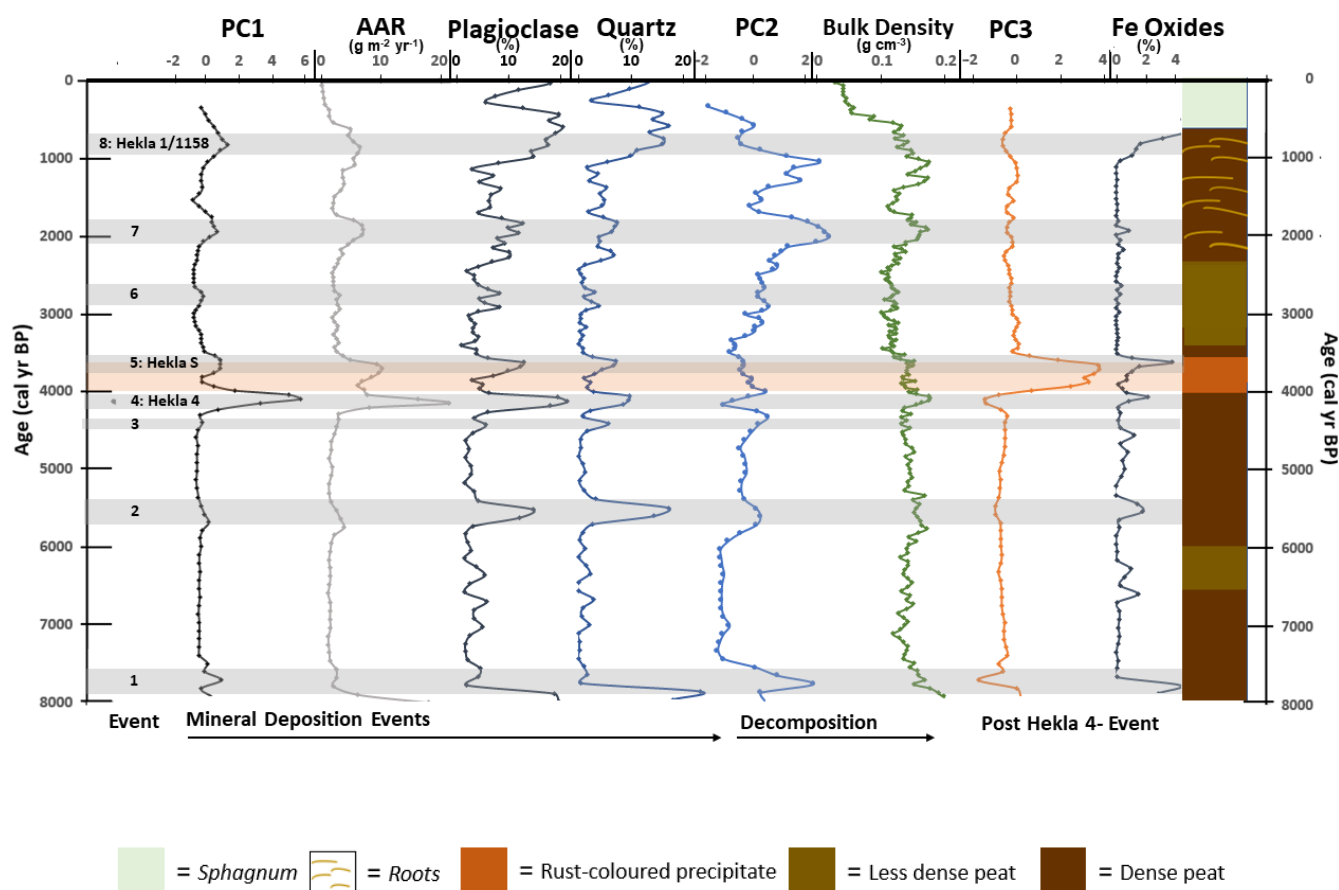


Figure 8. Summary of proxies discussed and interpretations. Grey bands represent identified mineral deposition events (Event 1-Event 8). The orange band represent an event associated with PC3.

6.4. Proxy Synthesis- Paleoenvironmental Summary

The peat sequence from Mýrarnar is characterized by at least 8 mineral deposition events where the inputs of lithogenic elements (PC1), plagioclase, quartz and Fe oxides are highly elevated. They are often associated with increases in decomposition (elevated PC2), which implies that the events have a fertilizing effect in the peat. In this section, these events will be discussed in a chronological order (Event 1- Event 8) along with changes in decomposition (PC2, bulk density) and events of another character (post Hekla 4 event, PC3) occurring in between them.

Around 8000 years ago the peat started to accumulate either by paludification over the saprolite or by terrestrialization over a pre-existing body of water, a common process in the Faroe Islands (Lawson et al., 2007). The latter is favoured here, as lakes (now a dammed reservoir) have been present on the Mýrarnar plateau into modern times while the Faroe Islands became progressively drier (Curtin et al., 2019). As previously discussed, the peat initiation at Mýrarnar is not attributed to a single climatic shift or event. Instead, peat started to accumulate according to local conditions (topography, hydrology, vegetation cover, soil development) as a long-term response to an earlier shift to a moist oceanic climate (Jóhansen, 1985; Hannon et al., 2003; 2010).

The first mineral deposition event (Event 1, Figure 8) occurs between 7900 and 7790 cal yr BP. The mineral input had a fertilising effect which increased the decomposition of the peat and followingly the retention of halogens (Biester et al., 2004) and Se in the peat, with Cu and Rb following a similar pattern (PC2). The lithogenic input of Event 1 could have several sources. It could be related to a low-concentration tephra layer dated to ~8000 cal yr BP, previously only identified in one peat core on the Faroe Islands (Wastegård, 2002). The layer possibly represents reworked tephra from earlier deposition (Wastegård et al., 2018), which means that Event 1 could represent a remobilizing storm event. The mineral deposition, regardless of tephra being present or not, could hence be sourced from increased aeolian and possibly fluvial activity associated with heavy storms. Another explanation could be the introduction of new source material allowing increased aeolian deposition, possibly derived from the Storegga tsunami that hit the Faroe Islands ~8000 cal yr BP (Grauert et al., 2001).

The period between Event 1 and Event 2 (~7790-5740 cal yr BP) has the lowest PC2 scores in the sequence, which implies that the peat decomposition is low. This is further suggested by the peat being visually less dense from ~6540 to ~6000 cal yr BP and the bulk density being lower than surrounding peat sections. A high water table would generate more comprehensive anoxic conditions and inhibit decomposition. It is therefore possible that this period saw wetter conditions prevail. The decomposition of the peat increases following fertilization (elevated PC2 scores) from the mineral deposition (elevated PC1 scores, plagioclase, quartz and Fe oxides) associated with Event 2 (~5740 cal yr BP). It is possible that this event is related to the deposition of two separate, but synchronous tephra layers recorded at one site in the Faroe Islands by Wastegård et al. (2001), dated to ~5900 cal yr BP. It is also possible that Event 2 is unrelated to tephra deposition and instead represents a period of increased storminess. The PC2 scores after Event 2 are higher than earlier in the sequence. This could be indicative of a shift to drier conditions promoting peat decomposition. The next event (Event 3, ~4440 cal yr BP) does not have any analogues in described tephra layers of the Faroe Islands (Wastegård et al., 2018). It could possibly represent a hitherto undescribed tephra deposition. Alternatively, it could represent a remobilisation of such or other lithogenic material following e.g., a storm event.

Event 4 (~4130 cal yr BP) is attributed to the deposition of the Hekla 4 tephra, which constitutes the most important deposition event of the sequence (ash content: 34.6%, AAR: 21.7 g m⁻² yr⁻¹). The event saw the deposition of volcanic glass (SEM-EDS and XRD analyses) but also plagioclase, quartz and Fe oxides (ATR-FTIR and XRD analyses). This indicates that the minerals either were deposited as a part of the tephra, and/or that the tephra deposition induced landscape changes that increased erosion and mineral deposition. One suggested mechanism is reduced vegetation cover following the widespread tephra deposition (Zobel and Antos, 1997). The Hekla 4 tephra provided a source of nutrients from whence Ca and Mn diffused upwards (PC4). This divides the sequence, as before Hekla 4 these elements are sourced from weathering of the underlying substrate.

Following Event 4 (Hekla 4) and through Event 5 (Hekla S), between ~3910 and ~3680 cal yr BP, the factor scores of PC3 are highly elevated. While increased erosion (Olsen et al., 2010; Lawson et al., 2007), decreased sea surface temperatures (Rasmussen and Thomsen, 2010) and vegetation shifts (Hannon et al., 2001; Lawson et al., 2008) suggest an intensified cooling in the Faroe Islands during this time, the event is here interpreted to represent upwards diffusion of components delivered with the Hekla 4 tephra. Upward relocation of Fe has previously been described following ash deposition events (Steinmann and Shotyk, 1997; Shotyk et al., 2005a). Hematite is present at least towards the end of the episode near Hekla S (~3740 cal yr BP), possibly indicating the presence of oxic conditions. The spherical shape of the hematite particle evokes a resemblance to that of Fe oxide concretions formed from mobilised iron precipitating in oxidising ground water (Busigny and Dauphas, 2007; Parry, 2011). It is therefore suggested that the Hekla 4 deposition possibly created a relatively impermeable layer towards the underlying peat, allowing a shallow pool of oxygenated water to cover the peat wherein the hematite could precipitate. This would be enhanced by increased surface runoff following either a coverage or reduction of vegetation cover. Further identification of the numerous diatoms found here during SEM-EDS analysis could aid in interpreting the prevailing conditions. The idea of Hekla 4 delineating or forming a barrier in the sequence is further suggested by the split in the diffusion profile of PC4 and a concurrent shift in PAR, bulk density and individual element profiles (Appendix B).

The peat becomes gradually more decomposed after Event 5 (Hekla S, ~3740 cal yr BP), potentially indicating a gradually drier climate as indicated by Curtin et al. (2019). Event 6 (~2800 cal yr BP) did seemingly not have a fertilizing effect in the peat. The event is possibly related to a Hekla 3 deposition (~3000 cal yr BP), which has been recorded at one site on the Faroe Islands (Olsen et al., 2010). A low concentration tephra layer was found at an undated but roughly corresponding depth in Mýrarnar by Persson (1968), possibly alluding to the presence of Hekla 3 in the profile. Again, this could however also be caused by a remobilisation of previously deposited tephra or other lithogenic material following e.g., a storm event.

Event 7 (~2000 cal yr BP) cannot be related to any known tephra horizons on the Faroe Islands (Wastegård et al., 2018). Hence, it could represent a hitherto undescribed direct deposition of tephra on the Faroe Islands. It is however concurrent with a period of greater storminess, reconstructed from a peat core from Islay, Scotland (Kylander et al., 2020). The deposition event could therefore also be that of a deposition of reworked tephra or minerals from storm events. After Event 7, between ~1700 and ~1380 cal yr BP, the degree of peat decomposition is low which could be indicative of temporary wetter conditions. After this period however, by ~1290 cal yr BP, the degree of decomposition is highly elevated. This is mirrored in the bulk density profile and PC2, but not in PC1. The period may therefore be characterised by dry conditions which caused a highly decomposed and compact peat, independent from lithogenic inputs. Around this time human colonisation of the Faroe Islands began (Hannon et al., 2001; 2005; Church et al., 2013; Curtin et al., 2021). The shift from a shrub to grass heath dominated vegetation possibly predating this colonisation (Hannon et al., 2005; Curtin et al., 2019) could be connected to the elevated decomposition rates. An anthropogenic forcing of the pattern is also possible. By ~1050 cal yr BP lithogenic inputs starts to increase (PC1, plagioclase and quartz) which potentially had a fertilizing effect in the peat, promoting the decomposition. The Tjörnuvík and Landnám tephra (~1150 and ~1070 cal yr BP) are recorded tephra layers at the Faroe Islands during this period (Wastegård et al., 2018) and could have provided the lithogenic input. The former is possibly a reworked tephra that could remobilise owing to increased erosion associated with the vegetation shift (Hannon et al. 2005; Curtin et al., 2019). Increasing rates of erosion on the Faroe Islands were also inferred at this time by Olsen et al. (2010) and Kylander et al. (2020) recorded increased storminess in Scotland. Whether the lithogenic input increase can be attributed to a climate induced increase in erosion, an anthropogenic impact or tephra deposition remains uncertain. The increase in lithogenic components culminates with the final event identified in the sequence, Event 8 (~820 cal yr BP). This event is attributed to the deposition of Hekla 1 and/or Hekla 1158, the input of which seemingly diluted the signal from PC2.

6.5. Implications and Future Prospects

The geochemical variability in the studied peat sequence is heavily characterised by several mineral deposition events throughout time. These events, represented by PC1, directly influence much of the variability seen in PC2 which is interpreted to represent retention of organically bound elements and accordingly decomposition (Biester et al., 2004). Furthermore, one of these deposition events, most probably being the Hekla 4 tephra deposition, is arguably the main feature of PC3 and PC4. The PC1 deposition events are further the principal mode of mineral input in the sequence. In other words, the events are the dominant source of the entire geochemical signal in the peat. To understand this signal, the characteristics of the deposition events need to be identified. While at least three of these events can

be attributed to tephra deposition (Hekla 4, Hekla S and Hekla 1/1158), the rest could not be identified within the timeframe of this thesis. Many of the events roughly align with known tephra horizons on the Faroe Islands (Wastegård et al., 2018) and it is possible that the geochemical signal of the sequence is completely dominated by tephra inputs. If this is the case, climate is a secondary controller on the geochemical signal and will be hard to interpret. Further identification of the mineral deposition events would be required to determine their character.

The identified tephtras are unique in being the only deposition events that do not entail an increase in PC2 (except possibly the mineral deposition event at ~2800 cal yr BP). This could be caused by their high AAR having a diluting effect on PC2 but would stand in contrast to the strongly correlated PC1 and PC2 peaks at ~2000 cal yr BP. It could instead be the result of different depositional patterns, where the non-identified events lead to more effective fertilisation than that of Hekla 4, Hekla S and Hekla 1/1158. Perhaps the unidentified events that have a positive correlation with PC2 peaks represent e.g., storm events with aeolian deposition containing more nutrients than tephra deposition events. While interesting, the notion that the relationship between the PC1 and PC2 peaks could help differentiate tephra deposition events from others cannot be proven here.

To improve the paleoenvironmental interpretation of the peat sequence, further analyses are proposed. The most important step would be to examine the character of the unidentified mineral deposition events. Confirming or denying the presence of tephra in corresponding peat sections would be instrumental in doing so. This could be done by further paired SEM-EDS and XRD analyses, or through density separation techniques (e.g. Turney, 1998). Any potential tephra with recorded analogues elsewhere, including the ones already identified, should be included in the age-depth model to constrain it further. They could furthermore be geochemically characterised to assess its provenance and whether it is a primary deposit or a reworked tephra. Because the latter would be affected by erosional processes, it is argued that it could contain climatic information. The retention of the elements associated with PC2 has here been argued to represent the rate of decomposition in the sequence. Generally, the decomposition increases with time which corroborates the result of Curtin et al. (2019) that the Faroese Holocene climate became increasingly dry with time. It is important to note here however that trend observed in this sequence is affected by the non-linear age model and that care needs to be taken when interpreting long-term change. To strengthen this interpretation independent analyses on peat decomposition are proposed. Available techniques include examining the C/N ratio (e.g. Kuhry and Vitt, 1996) and spectral data from FTIR (e.g. Martínez Cortizas et al., 2021b).

The oceanic Faroe Islands presents ideal conditions for studying past climates, where important North Atlantic climate mechanisms such as the AMOC and NAO governs large and human influence has been minimal. Theoretically, this makes the islands highly interesting in inferring climate variation in a wider

Nort Atlantic context. To widen and improve the existing knowledge on Faroese paleoenvironments, it is arguably important to compliment the currently biological proxy- and lacustrine dominated studies with e.g., geochemical proxies of peat. However, the temporally compressed records and the possibility of a complete dominance of tephra in the geochemical signal complicate such paleoclimatic interpretations. As at least three of the major peaks in the lithogenic geochemical signal are heavily characterized by tephra, there is a possibility that this is also the case for all such signals. Hence, the elemental geochemistry signal will many times not be climate related which alone deems it insufficient in representing climate variability. This stresses the need for using complimentary analyses allowing mineral identification (e.g. XRD, SEM-EDS and ATR-FTIR) when conducting paleoenvironmental studies using elemental geochemistry. Tephra is generally widely dispersed and affect large areas. If tephra is not considered and identified in areas prone to tephra deposition, climatic interpretations based on geochemistry might be incorrect.

The possible dominance of volcanic signals in the peat sequence further evokes an interesting discussion on how to disentangle climatic signals in geochemistry from volcanically dominated areas. If indeed every identified mineral event in this study is dominated by tephra, it is evident that robust methods need to be developed to differentiate volcanic signals from climatic ones. This is especially true given the tendency of tephra being remobilized in a setting like the Faroe Islands (Wastegård et al., 2018), as it could be difficult to differentiate between a primary (volcanic signal) and a secondary deposition (climatic signal). Suggestions on future directions include identifying compositional differences between local aeolian and volcanically derived material. Whether containing reworked tephra or not, aeolian deposition is suspected to contain non-tephra components. Examining ratios of elements or minerals unique to the source (Le Roux et al., 2012) could hence possibly differentiate primary tephra deposition from aeolian deposition. The rounded quartz grains found in some samples in this study could further potentially be used as indicators of aeolian transported material. It is possible that the large variations caused by the mineral deposition events leads to some weaknesses in using PCA to interpret the data. This is because the mineral deposition events dominate the statistical output which means that other processes might be difficult to detect. With this reasoning, individual element profiles and ratios between them could potentially capture processes not captured by the PCA. Using alternative methods to explore the dataset and associations therein is therefore proposed as a potential future prospect. Lastly, it is suggested that further work on isolating the tephra signal in ATR-FTIR (see above) is done. If the tephra spectra can be differentiated to various mineral spectra, their respective behaviour throughout the sequence could be traced.

Conclusion

By examining elemental geochemistry and linking it with mineralogy and physical proxies in a peat core from Mýrarnar, the Faroe Islands, mineral deposition and peat decomposition throughout the last ~8000 years have been reconstructed. A period of weak peat decomposition is inferred from ~7500 to ~6000 cal yr BP, after which it generally increases towards the top of the sequence. This possibly represents the climate gradually becoming drier with time. At least 8 mineral deposition events are identified, with peaks dated to 7790, 5740, 4440, 4130, 3740, 2800, 1960 and 820 cal yr BP. Many of these events are associated with a fertilization in the peat and strengthened decomposition. At least three of the events are characterized by tephra and can be temporally aligned with the previously described Faroese tephra horizons of Hekla 4 (4130 cal yr BP), Hekla S (3740 cal yr BP) and Hekla 1 and/or Hekla 1158 (820 cal yr BP) (Wastegård et al., 2018). The character of the remaining mineral deposition events is unknown and further identification of these events is proposed. With the possibility of every mineral deposition event being related to tephra, techniques differentiating primary (volcanic signal) and secondary tephra (climatic signal) deposition need to be examined to extract geochemical climatic signals from the paleoclimatically interesting Faroe Islands.

Acknowledgements

First and foremost, I would like to thank my supervisors Dr. Malin Kylander and Dr. Jenny Sjöström for your incredible support, dedication and enthusiasm throughout the whole process. Thank you for giving me the opportunity to work on this project and for introducing me to the methodology. Most of all, thank you for being so inviting and letting me be a part of your fantastic team.

Many thanks are extended to Carina Johansson for your support and enthusiasm. Your help during laboratory work has been invaluable. Prof. Antonio Martínez Cortizas and Dr. Mohamed Traoré are thanked for performing the WD-XRF analysis at the University of Santiago de Compostela. Prof. Antonio Martínez Cortizas is further thanked for the performing the reduction and interpretation of the ATR-FTIR data used in this thesis as well as providing valuable feedback. Thank you, Eleonor Ryberg, for your support in identifying plant macrofossils picked for radiocarbon dating. Andreas Karlsson at the Swedish museum of Natural History is thanked for valuable support during XRD and SEM-EDS analyses. Many thanks to Dr. Daniel Ellerton and Prof. Richard Bindler for rewarding discussions and for sharing your knowledge, both during and after the field campaign. Lastly, I extend my thanks to the Bolin Centre for Climate Research for helping me fund this project.



References

- Álvarez Fernández, N., Martínez Cortizas, A., 2020. Andurinha Make Spectroscopic Data Processing Easier. R package version 0.0. Available online: https://CRAN.Rproject.org/package_andurinha.2020 (accessed on 4 May 2022).
- Andresen, C.S., Björck, S., Jessen, C. and Rundgren, M., 2007. Early Holocene terrestrial climatic variability along a North Atlantic Island transect: palaeoceanographic implications. *Quaternary Science Reviews*, 26(15-16), pp.1989-1998.
- Andresen, C.S., Björck, S., Rundgren, M., Conley, D.J. and Jessen, C., 2006. Rapid Holocene climate changes in the North Atlantic: evidence from lake sediments from the Faroe Islands. *Boreas*, 35(1), pp.23-34.
- Andrews, J.T., Eberl, D.D. and Kristjansdottir, G.B., 2006. An exploratory method to detect tephras from quantitative XRD scans: examples from Iceland and east Greenland marine sediments. *The Holocene*, 16(8), pp.1035-1042.
- Arge, S.V., Sveinbjarnardóttir, G., Edwards, K.J. and Buckland, P.C., 2005. Viking and medieval settlement in the Faroes: people, place and environment. *Human Ecology*, 33(5), pp.597-620.
- Barber, K.E., Chambers, F.M. and Maddy, D., 2003. Holocene palaeoclimates from peat stratigraphy: macrofossil proxy climate records from three oceanic raised bogs in England and Ireland. *Quaternary Science Reviews*, 22(5-7), pp.521-539.
- Bergerhoff, G., Brown, I.D. and Allen, F., 1987. Crystallographic databases. *International Union of Crystallography, Chester*, 360, pp.77-95.
- Biester, H., Keppler, F., Putschew, A., Martinez-Cortizas, A. and Petri, M., 2004. Halogen retention, organohalogens, and the role of organic matter decomposition on halogen enrichment in two Chilean peat bogs. *Environmental science & technology*, 38(7), pp.1984-1991.
- Biester, H., Selimović, D., Hemmerich, S. and Petri, M., 2006. Halogens in pore water of peat bogs—the role of peat decomposition and dissolved organic matter. *Biogeosciences*, 3(1), pp.53-64.
- Bindler, R., 2006. Mired in the past—looking to the future: geochemistry of peat and the analysis of past environmental changes. *Global and Planetary change*, 53(4), pp.209-221.
- Bindler, R., Klarqvist, M., Klaminder, J. and Förster, J., 2004. Does within-bog spatial variability of mercury and lead constrain reconstructions of absolute deposition rates from single peat records? The example of Store Mosse, Sweden. *Global Biogeochemical Cycles*, 18(3).
- Birks, H.J.B., 1981. The use of pollen analysis in the reconstruction. *Climate and history: studies in past climates and their impact on man*, p.111.
- Björck, S. and Clemmensen, L.B., 2004. Aeolian sediment in raised bog deposits, Halland, SW Sweden: a new proxy record of Holocene winter storminess variation in southern Scandinavia?. *The Holocene*, 14(5), pp.677-688.

- Björck, S., Muscheler, R., Kromer, B., Andresen, C.S., Heinemeier, J., Johnsen, S.J., Conley, D., Koç, N., Spurk, M. and Veski, S., 2001. High-resolution analyses of an early Holocene climate event may imply decreased solar forcing as an important climate trigger. *Geology*, 29(12), pp.1107-1110.
- Blackford, J., 2000. Palaeoclimatic records from peat bogs. *Trends in Ecology & Evolution*, 15(5), pp.193-198.
- Blaauw, M. and Christen, J.A., 2011. Flexible paleoclimate age-depth models using an autoregressive gamma process. *Bayesian analysis*, 6(3), pp.457-474.
- Blytt, A., 1876. *Essay on the immigration of the Norwegian flora during alternating rainy and dry periods*. A. Cammermeyer.
- Boyle, J., 2001. Redox remobilization and the heavy metal record in lake sediments: a modelling approach. *Journal of Paleolimnology*, 26(4), pp.423-431.
- Broder, T., Blodau, C., Biester, H. and Knorr, K.H., 2012. Peat decomposition records in three pristine ombrotrophic bogs in southern Patagonia. *Biogeosciences*, 9(4), pp.1479-1491.
- Buckley, M.W. and Marshall, J., 2016. Observations, inferences, and mechanisms of the Atlantic Meridional Overturning Circulation: A review. *Reviews of Geophysics*, 54(1), pp.5-63.
- Busigny, V. and Dauphas, N., 2007. Tracing paleofluid circulations using iron isotopes: A study of hematite and goethite concretions from the Navajo Sandstone (Utah, USA). *Earth and Planetary Science Letters*, 254(3-4), pp.272-287.
- Caesar, L., McCarthy, G.D., Thornalley, D.J.R., Cahill, N. and Rahmstorf, S., 2021. Current Atlantic meridional overturning circulation weakest in last millennium. *Nature Geoscience*, 14(3), pp.118-120.
- Canada Soil Survey Committee, 1978. *The Canadian system of soil classification*. Research Branch, Canada Department of Agriculture.
- Cappelen, J., 2020. *The Faroe Islands-DMI Historical Climate Data Collection 1873-2019*. Danish Meteorological Institute.
- Cappelen, J. and Laursen, E.V., 1998. *The Climate of the Faroe Islands-with climatological standard normals, 1961-1990*. DMI.
- Cattell, R.B., 1966. The scree test for the number of factors. *Multivariate behavioral research*, 1(2), pp.245-276.
- Chambers, F.M., Beilman, D.W. and Yu, Z., 2011. Methods for determining peat humification and for quantifying peat bulk density, organic matter and carbon content for palaeostudies of climate and peatland carbon dynamics. *Mires and Peat*, 7(7), pp.1-10.
- Chambers, F.M., Booth, R.K., De Vleeschouwer, F., Lamentowicz, M., Le Roux, G., Mauquoy, D., Nichols, J.E. and Van Geel, B., 2012. Development and refinement of proxy-climate indicators from peats. *Quaternary International*, 268, pp.21-33.

- Chambers, F.M. and Charman, D.J., 2004. Holocene environmental change: contributions from the peatland archive. *The Holocene*, 14(1), pp.1-6.
- Chen, D., Rojas, M., Samset, B.H., Cobb, K., Diongue Niang, A., Edwards, P., Emori, S., Faria, S.H., Hawkins, E., Hope, P., Huybrechts, P., Meinshausen, M., Mustafa, S.K., Plattner, G.-K. and Tréguier, A.-M., 2021: Framing, Context, and Methods. In *Climate Change 2021: The Physical Science Basis. Contribution of Working Group I to the Sixth Assessment Report of the Intergovernmental Panel on Climate Change* [Masson-Delmotte, V., Zhai, P., Pirani, A., Connors, S.L., Péan, C., Berger, S., Caud, N., Chen, Y., Goldfarb, L., Gomis, M.I., Huang, M., Leitzell, K., Lonnoy, E., Matthews, J.B.R., Maycock, T.K., Waterfield, T., Yelekçi, O., Yu, R. and Zhou, B. (eds.)]. Cambridge University Press, Cambridge, United Kingdom and New York, NY, USA, pp. 147–286, doi:10.1017/9781009157896.003.
- Chesworth, W., Cortizas, A.M. and García-Rodeja, E., 2006. The redox–pH approach to the geochemistry of the Earth's land surface, with application to peatlands. *Developments in Earth surface processes*, 9, pp.175-195.
- Church, M.J., Arge, S.V., Brewington, S., McGovern, T.H., Woollett, J.M., Perdikaris, S., Lawson, I.T., Cook, G.T., Amundsen, C., Harrison, R. and Krivogorskaya, Y., 2005. Puffins, pigs, cod and barley: palaeoeconomy at Undir Junkarinsfløtti, Sandoy, Faroe Islands. *Environmental Archaeology*, 10(2), pp.179-197.
- Church, M.J., Arge, S.V., Edwards, K.J., Ascough, P.L., Bond, J.M., Cook, G.T., Dockrill, S.J., Dugmore, A.J., McGovern, T.H., Nesbitt, C. and Simpson, I.A., 2013. The Vikings were not the first colonizers of the Faroe Islands. *Quaternary Science Reviews*, 77, pp.228-232.
- Christiansen, H.H., 1998. Highland aeolian deposits in the Faroe Islands. *Fróðskaparrit*, 46, pp.205-213.
- Christiansen, H.H. and Humlum, O., 2003. The southern boundary of the Northern Hemisphere periglacial zone at the Faroe Islands. In *Phillips, M., Springman, SM, and Arenson, LU, Proceedings of the 8th International Conference on Permafrost, Zurich. AA Balkema, Lisse* (pp. 139-144).
- Christiansen, H.H. & Mortensen, L.E., 2002. Arctic Mountain Meteorology at the Sornfelli Mountain in Year 2000 in the Faroe Islands. *Fróðskaparrit* 50, 93–110.
- Curtin, L., D'Andrea, W.J., Balascio, N., Pugsley, G., de Wet, G. and Bradley, R., 2019. Holocene and Last Interglacial climate of the Faroe Islands from sedimentary plant wax hydrogen and carbon isotopes. *Quaternary Science Reviews*, 223, p.105930.
- Curtin, L., D'Andrea, W.J., Balascio, N.L., Shirazi, S., Shapiro, B., de Wet, G.A., Bradley, R.S. and Bakke, J., 2021. Sedimentary DNA and molecular evidence for early human occupation of the Faroe Islands. *Communications Earth & Environment*, 2(1), pp.1-7.
- Crawford, R.M.M., 2000. Ecological hazards of oceanic environments. *New Phytologist*, 147(2), pp.257-281.

- de Jong, R., Björck, S., Björkman, L. and Clemmensen, L.B., 2006. Storminess variation during the last 6500 years as reconstructed from an ombrotrophic peat bog in Halland, southwest Sweden. *Journal of Quaternary Science: Published for the Quaternary Research Association*, 21(8), pp.905-919.
- Dean, W.E. 1974. Determination of carbonate and organic matter in calcareous sediments and sedimentary rocks by loss on ignition: comparison with other methods. *Journal of Sedimentary Research* 44(1), pp.242–8
- Deser, C., Hurrell, J.W. and Phillips, A.S., 2017. The role of the North Atlantic Oscillation in European climate projections. *Climate dynamics*, 49(9), pp.3141-3157.
- Edwards, K.J., Borthwick, D., Cook, G., Dugmore, A.J., Mairs, K.A., Church, M.J., Simpson, I.A. and Adderley, W.P., 2005. A hypothesis-based approach to landscape change in Suðuroy, Faroe Islands. *Human Ecology*, 33(5), pp.621-650.
- Faust, J.C., Fabian, K., Milzer, G., Giraudeau, J. and Knies, J., 2016. Norwegian fjord sediments reveal NAO related winter temperature and precipitation changes of the past 2800 years. *Earth and Planetary Science Letters*, 435, pp.84-93.
- Feser, F., Barcikowska, M., Krueger, O., Schenk, F., Weisse, R. and Xia, L., 2015. Storminess over the North Atlantic and northwestern Europe—A review. *Quarterly Journal of the Royal Meteorological Society*, 141(687), pp.350-382.
- Fox-Kemper, B., Hewitt, H.T., Xiao, C., Aðalgeirsdóttir, G., Drijfhout, S.S., Edwards, T.L., Golledge, N.R., Hemer, M., Kopp, R.E., Krinner, G., Mix, A., Notz, D., Nowicki, S., Nurhati, I.S., Ruiz, L., Sallée, J.-B., Slangen, A.B.A. and Yu, Y., 2021: Ocean, Cryosphere and Sea Level Change. In *Climate Change 2021: The Physical Science Basis. Contribution of Working Group I to the Sixth Assessment Report of the Intergovernmental Panel on Climate Change* [Masson-Delmotte, V., Zhai, P., Pirani, A., Connors, S.L., Péan, C., Berger, S., Caud, N., Chen, Y., Goldfarb, L., Gomis, M.I., Huang, M., Leitzell, K., Lonnoy, E., Matthews, J.B.R., Maycock, T.K., Waterfield, T., Yelekçi, O., Yu, R. and Zhou, B. (eds.)]. Cambridge University Press, Cambridge, United Kingdom and New York, NY, USA, pp. 1211–1362, doi:10.1017/9781009157896.011.
- Friedman, I. and Long, W., 1984. Volcanic glasses, their origins and alteration processes. *Journal of Non-Crystalline Solids*, 67(1-3), pp.127-133.
- Gillett, N.P., Graf, H.F. and Osborn, T.J., 2003. Climate change and the North Atlantic oscillation. *Geophysical Monograph-American Geophysical Union*, 134, pp.193-210.
- Gimingham, C.H., 1964. Dwarf shrub heaths. *The vegetation of Scotland*, 232.
- Gorham, E., 1957. The development of peat lands. *The Quarterly Review of Biology*, 32(2), pp.145-166.
- Grauert, M., Börck, S. and Bondevik, S., 2001. Storegga tsunami deposits in a coastal lake on Suðuroy, the Faroe Islands. *Boreas*, 30(4), pp.263-271.

- Gribble, G.W., 2003. The diversity of naturally produced organohalogenes. *Chemosphere*, 52(2), pp.289-297.
- Hannon, G.E. and Bradshaw, R.H., 2000. Impacts and timing of the first human settlement on vegetation of the Faroe Islands. *Quaternary Research*, 54(3), pp.404-413.
- Hannon, G.E., Bradshaw, R.H., Bradshaw, E.G., Snowball, I. and Wastegård, S., 2005. Climate change and human settlement as drivers of late-Holocene vegetational change in the Faroe Islands. *The Holocene*, 15(5), pp.639-647.
- Hannon, G.E., Bradshaw, R.H. and Wastegård, S., 2003. Rapid vegetation change during the early Holocene in the Faroe Islands detected in terrestrial and aquatic ecosystems. *Journal of Quaternary Science*, 18(7), pp.615-619.
- Hannon, G.E., Rundgren, M. and Jessen, C.A., 2010. Dynamic early Holocene vegetation development on the Faroe Islands inferred from high-resolution plant macrofossil and pollen data. *Quaternary Research*, 73(2), pp.163-172.
- Hannon, G.E., Wastegård, S., Bradshaw, E. and Bradshaw, R.H., 2001, December. Human impact and landscape degradation on the Faroe Islands. In *Biology and Environment: Proceedings of the Royal Irish Academy* (pp. 129-139). Royal Irish Academy.
- Hansen, K. & Jóhansen, J., 1982. Flora and vegetation of the Faeroe Islands. In: Rutherford, G. K. (ed.) *The physical environment of the Faeroe Islands*, Monographiae Biologicae 46. Junk Publishers, The Hague, NL pp.35-52.
- Harning, D.J., Thordarson, T., Geirsdóttir, Á., Zalzal, K. and Miller, G.H., 2018. Provenance, stratigraphy and chronology of Holocene tephra from Vestfirðir, Iceland. *Quaternary Geochronology*, 46, pp.59-76.
- Holmes, A., 1918. The basaltic rocks of the Arctic region. *Mineralogical magazine and journal of the Mineralogical Society*, 18(85), pp.180-223.
- Humlum, O. and Christiansen, H.H., 1998. Mountain climate and periglacial phenomena in the Faeroe Islands. *Permafrost and periglacial processes*, 9(3), pp.189-211.
- Hurrell, J.W., 1995. Decadal trends in the North Atlantic Oscillation: Regional temperatures and precipitation. *Science*, 269(5224), pp.676-679.
- Hurrell, J.W. and Deser, C., 2010. North Atlantic climate variability: the role of the North Atlantic Oscillation. *Journal of marine systems*, 79(3-4), pp.231-244.
- Hurrell, J.W. and Loon, H.V., 1997. Decadal variations in climate associated with the North Atlantic Oscillation. In *Climatic change at high elevation sites*. Springer, Dordrecht, pp. 69-94.
- Jessen, C.A., Rundgren, M., Björck, S., Andresen, C.S. and Conley, D.J., 2008. Variability and seasonality of North Atlantic climate during the early Holocene: evidence from Faroe Island lake sediments. *The Holocene*, 18(6), pp.851-860.
- Jóhansen, J. 1985. *Studies in the Vegetational History of the Faroe and Shetland Islands*. Annales Societatis Scientiarum Faeroensis Supplementum XI, Tórshavn.

- Kuhlbrodt, T., Griesel, A., Montoya, M., Levermann, A., Hofmann, M. and Rahmstorf, S., 2007. On the driving processes of the Atlantic meridional overturning circulation. *Reviews of Geophysics*, 45(2).
- Kuhry, P. and Turunen, J., 2006. The postglacial development of boreal and subarctic peatlands. In *Boreal peatland ecosystems*. Springer, Berlin, Heidelberg, pp. 25-46.
- Kuhry, P. and Vitt, D.H., 1996. Fossil carbon/nitrogen ratios as a measure of peat decomposition. *Ecology*, 77(1), pp.271-275.
- Kylander, M.E., Bindler, R., Martínez Cortizas, A., Gallagher, K., Mörth, C.M. and Rauch, S., 2013. A novel geochemical approach to paleorecords of dust deposition and effective humidity: 8500 years of peat accumulation at Store Mosse (the “Great Bog”), Sweden. *Quaternary Science Reviews*, 69, pp.69-82.
- Kylander, M.E., Holm, M., Fitchett, J., Grab, S., Martinez Cortizas, A., Norström, E. and Bindler, R., 2021. Late glacial (17,060–13,400 cal yr BP) sedimentary and paleoenvironmental evolution of the Sekhokong Range (Drakensberg), southern Africa. *Plos one*, 16(3), p.e0246821.
- Kylander, M.E., Martínez Cortizas, A., Bindler, R., Greenwood, S.L., Mörth, C.M. and Rauch, S., 2016. Potentials and problems of building detailed dust records using peat archives: An example from Store Mosse (the “Great Bog”), Sweden. *Geochimica et cosmochimica acta*, 190, pp.156-174.
- Kylander, M.E., Martínez-Cortizas, A., Bindler, R., Kaal, J., Sjöström, J.K., Hansson, S.V., Silva-Sánchez, N., Greenwood, S.L., Gallagher, K., Rydberg, J. and Mörth, C.M., 2018. Mineral dust as a driver of carbon accumulation in northern latitudes. *Scientific reports*, 8(1), pp.1-10.
- Kylander, M.E., Muller, J., Wüst, R.A.J., Gallagher, K., Garcia-Sanchez, R., Coles, B.J. and Weiss, D.J., 2007. Rare earth element and Pb isotope variations in a 52 kyr peat core from Lynch’s Crater (NE Queensland, Australia): Proxy development and application to paleoclimate in the Southern Hemisphere. *Geochimica et Cosmochimica Acta*, 71(4), pp.942-960.
- Kylander, M.E., Söderlindh, J., Schenk, F., Gyllencreutz, R., Rydberg, J., Bindler, R., Martínez Cortizas, A. and Skelton, A., 2020. It’s in your glass: a history of sea level and storminess from the Laphroaig bog, Islay (southwestern Scotland). *Boreas*, 49(1), pp.152-167.
- Kylander, M.E., Weiss, D.J., Cortizas, A.M., Spiro, B., Garcia-Sanchez, R. and Coles, B.J., 2005. Refining the pre-industrial atmospheric Pb isotope evolution curve in Europe using an 8000 year old peat core from NW Spain. *Earth and Planetary Science Letters*, 240(2), pp.467-485.
- Lafuente, B., Downs, R.T., Yang, H. and Stone, N., 2015. 1. The power of databases: The RRUFF project. In *Highlights in mineralogical crystallography* (pp. 1-30). De Gruyter (O).
- Lawson, I.T., Church, M.J., Edwards, K.J., Cook, G.T. and Dugmore, A.J., 2007. Peat initiation in the Faroe Islands: climate change, pedogenesis or human impact?. *Earth and Environmental Science Transactions of the Royal Society of Edinburgh*, 98(1), pp.15-28.

- Lawson, I.T., Church, M.J., McGovern, T.H., Arge, S.V., Woollet, J., Edwards, K.J., Gathorne-Hardy, F.J., Dugmore, A.J., Cook, G., Mairs, K.A. and Thomson, A.M., 2005. Historical ecology on Sandoy, Faroe Islands: palaeoenvironmental and archaeological perspectives. *Human Ecology*, 33(5), pp.651-684.
- Lawson, I.T., Edwards, K.J., Church, M.J., Newton, A.J., Cook, G.T., Gathorne-Hardy, F.J. and Dugmore, A.J., 2008. Human impact on an island ecosystem: pollen data from Sandoy, Faroe Islands. *Journal of Biogeography*, 35(6), pp.1130-1152.
- Le Roux, G., Fagel, N., De Vleeschouwer, F., Krachler, M., Debaille, V., Stille, P., Mattielli, N., Van Der Knaap, W.O., Van Leeuwen, J.F. and Shotyk, W., 2012. Volcano-and climate-driven changes in atmospheric dust sources and fluxes since the Late Glacial in Central Europe. *Geology*, 40(4), pp.335-338.
- Lee, J.-Y., Marotzke, J., Bala, G., Cao, L., Corti, S., Dunne, J.P., Engelbrecht, F., Fischer, E., Fyfe, J.C., Jones, C., Maycock, A., Mutemi, J., Ndiaye, O., Panickal, S. and Zhou T., 2021: Future Global Climate: Scenario-Based Projections and Near-Term Information. In *Climate Change 2021: The Physical Science Basis. Contribution of Working Group I to the Sixth Assessment Report of the Intergovernmental Panel on Climate Change* [Masson-Delmotte, V., Zhai, P., Pirani, A., Connors, S.L., Péan, C., Berger, S., Caud, N., Chen, Y., Goldfarb, L., Gomis, M.I., Huang, M., Leitzell, K., Lonnoy, E., Matthews, J.B.R., Maycock, T.K., Waterfield, T., Yelekçi, O., Yu, R. and Zhou, B. (eds.)]. Cambridge University Press, Cambridge, United Kingdom and New York, NY, USA, pp. 553–672, doi:10.1017/9781009157896.006.
- Marcott, S.A., Shakun, J.D., Clark, P.U. and Mix, A.C., 2013. A reconstruction of regional and global temperature for the past 11,300 years. *Science*, 339(6124), pp.1198-1201.
- Marshall, J., Kushnir, Y., Battisti, D., Chang, P., Czaja, A., Dickson, R., Hurrell, J., McCartney, M., Saravanan, R. and Visbeck, M., 2001. North Atlantic climate variability: phenomena, impacts and mechanisms. *International Journal of Climatology: A Journal of the Royal Meteorological Society*, 21(15), pp.1863-1898.
- Martínez Cortizas, A., Biester, H., Mighall, T. and Bindler, R., 2007. Climate-driven enrichment of pollutants in peatlands. *Biogeosciences*, 4(5), pp.905-911.
- Martínez Cortizas, A., Garcia-Rodeja, E., Pombal, X.P., Muñoz, J.N., Weiss, D. and Cheburkin, A., 2002. Atmospheric Pb deposition in Spain during the last 4600 years recorded by two ombrotrophic peat bogs and implications for the use of peat as archive. *Science of the Total Environment*, 292(1-2), pp.33-44.
- Martínez Cortizas, A., López-Costas, O., Orme, L., Mighall, T., Kylander, M.E., Bindler, R. and Gallego Sala, Á., 2020. Holocene atmospheric dust deposition in NW Spain. *The Holocene*, 30(4), pp.507-518.

- Martínez Cortizas, A., López-Merino, L., Silva-Sánchez, N., Sjöström, J.K. and Kylander, M.E., 2021(a). Investigating the Mineral Composition of Peat by Combining FTIR-ATR and Multivariate Analysis. *Minerals*, *11*(10), p.1084.
- Martínez Cortizas, A., Pontevedra-Pombal, X., Garcia-Rodeja, E., Novoa-Munoz, J.C. and Shotyk, W., 1999. Mercury in a Spanish peat bog: archive of climate change and atmospheric metal deposition. *Science*, *284*(5416), pp.939-942.
- Martínez Cortizas, A., Pontevedra-Pombal, X., Munoz, J.C. and García-Rodeja, E., 1997. Four thousand years of atmospheric Pb, Cd and Zn deposition recorded by the ombrotrophic peat bog of Penido Vello (Northwestern Spain). *Water, air, and soil pollution*, *100*(3), pp.387-403.
- Martínez Cortizas, A., Sjöström, J.K., Ryberg, E.E., Kylander, M.E., Kaal, J., López-Costas, O., Álvarez Fernández, N. and Bindler, R., 2021(b). 9000 years of changes in peat organic matter composition in Store Mosse (Sweden) traced using FTIR-ATR. *Boreas*, *50*(4), pp.1161-1178.
- Martínez Cortizas, A., Vázquez, C.F., Kaal, J., Biester, H., Casais, M.C., Rodríguez, T.T. and Lado, L.R., 2016. Bromine accumulation in acidic black colluvial soils. *Geochimica et Cosmochimica Acta*, *174*, pp.143-155.
- Mauquoy, D. and Van Geel, B., 2007. Plant macrofossil methods and studies: mire and peat macros. In *Encyclopedia of quaternary science* (pp. 2315-2336). Elsevier Science.
- McKenna, C.M. and Maycock, A.C., 2021. Sources of Uncertainty in Multimodel Large Ensemble Projections of the Winter North Atlantic Oscillation. *Geophysical Research Letters*, *48*(14), p.e2021GL093258.
- McKenzie, J.M., Siegel, D.I., Shotyk, W., Steinmann, P. and Pfunder, G., 2002. Heuristic numerical and analytical models of the hydrologic controls over vertical solute transport in a domed peat bog, Jura Mountains, Switzerland. *Hydrological Processes*, *16*(5), pp.1047-1064.
- McLaren, R.G. and Crawford, D.V., 1973. Studies on soil copper: II. the specific adsorption of copper by soils. *Journal of soil science*, *24*(4), pp.443-452.
- Meara, R.H., Thordarson, T.H., Pearce, N.J.G., Hayward, C. and Larsen, G., 2020. A catalogue of major and trace element data for Icelandic Holocene silicic tephra layers. *Journal of Quaternary Science*, *35*(1-2), pp.122-142.
- Muller, J., Kylander, M., Martínez Cortizas, A., Wüst, R.A., Weiss, D., Blake, K., Coles, B. and Garcia-Sanchez, R., 2008. The use of principle component analyses in characterising trace and major elemental distribution in a 55 kyr peat deposit in tropical Australia: Implications to paleoclimate. *Geochimica et Cosmochimica Acta*, *72*(2), pp.449-463.
- Nesje, A., Lie, Ø. and Dahl, S.O., 2000. Is the North Atlantic Oscillation reflected in Scandinavian glacier mass balance records?. *Journal of Quaternary Science: Published for the Quaternary Research Association*, *15*(6), pp.587-601.

- Nielsen, T., Rasmussen, T.L., Ceramicola, S. and Kuijpers, A., 2007. Quaternary sedimentation, margin architecture and ocean circulation variability around the Faroe Islands, North Atlantic. *Quaternary Science Reviews*, 26(7-8), pp.1016-1036.
- Olsen, J., Anderson, N.J. and Knudsen, M.F., 2012. Variability of the North Atlantic Oscillation over the past 5,200 years. *Nature Geoscience*, 5(11), pp.808-812.
- Olsen, J., Björck, S., Leng, M.J., Gudmundsdóttir, E.R., Odgaard, B.V., Lutz, C.M., Kendrick, C.P., Andersen, T.J. and Seidenkrantz, M.S., 2010. Lacustrine evidence of Holocene environmental change from three Faroese lakes: a multiproxy XRF and stable isotope study. *Quaternary Science Reviews*, 29(19-20), pp.2764-2780.
- Orme, L.C., Charman, D.J., Reinhardt, L., Jones, R.T., Mitchell, F.J., Stefanini, B.S., Barkwith, A., Ellis, M.A. and Grosvenor, M., 2017. Past changes in the North Atlantic storm track driven by insolation and sea-ice forcing. *Geology*, 45(4), pp.335-338.
- Orme, L.C., Davies, S.J. and Duller, G.A.T., 2015. Reconstructed centennial variability of late Holocene storminess from Cors Fochno, Wales, UK. *Journal of Quaternary Science*, 30(5), pp.478-488.
- Rasmussen, J., 1982. The Faeroe Islands: Geology. In Rutherford, G. K. (ed.), *The Physical Environment of the Faeroe Islands*, Monographiae Biologicae 46, Junk Publishers, The Hague, pp. 13–34.
- Rasmussen, J. and Noe-Nygaard, A., 1970. Geology of the Faroe Islands, Danmarks Geologiske Undersøgelser I, serie 25.
- Rasmussen, T.L. and Thomsen, E., 2010. Holocene temperature and salinity variability of the Atlantic Water inflow to the Nordic seas. *The Holocene*, 20(8), pp.1223-1234.
- Reimer, P.J., Austin, W.E., Bard, E., Bayliss, A., Blackwell, P.G., Ramsey, C.B., Butzin, M., Cheng, H., Edwards, R.L., Friedrich, M. and Grootes, P.M., 2020. The IntCal20 Northern Hemisphere radiocarbon age calibration curve (0–55 cal kBP). *Radiocarbon*, 62(4), pp.725-757.
- Reintges, A., Martin, T., Latif, M. and Keenlyside, N.S., 2017. Uncertainty in twenty-first century projections of the Atlantic Meridional Overturning Circulation in CMIP3 and CMIP5 models. *Climate Dynamics*, 49(5), pp.1495-1511.
- Renberg, I., Persson, M.W. and Emteryd, O., 1994. Pre-industrial atmospheric lead contamination detected in Swedish lake sediments. *Nature*, 368(6469), pp.323-326.
- Rutherford G.K., Taylor C.E.B., 1982 (a). Location and General Description. In: Rutherford G.K. (ed.), *The Physical Environment of the Faeroe Islands*. Monographiae Biologicae 46, Junk Publishers, The Hague, pp.3–15.
- Rutherford G.K., Taylor C.E.B., 1982 (b). Soils of the Faroe Islands. In: Rutherford G.K. (ed.), *The Physical Environment of the Faeroe Islands*. Monographiae Biologicae 46, Junk Publishers, The Hague, pp.111–124.

- Rydin, H., Gunnarsson, U. and Sundberg, S., 2006. The role of Sphagnum in peatland development and persistence. In *Boreal peatland ecosystems*. Springer, Berlin, Heidelberg, pp. 47-65.
- Parry, W.T., 2011. Composition, nucleation, and growth of iron oxide concretions. *Sedimentary Geology*, 233(1-4), pp.53-68.
- Persson, C., 1968. Försök till tefrokronologisk datering i fyra färöiska myrar. *Geologiska Föreningen i Stockholm Förhandlingar*, 90(2), pp.241-266.
- Porter, C., Morin, P., Howat, I., Noh, M.-J., Bates, B., Peterman, K., Keeseey, S., Schlenk, M., Gardiner, J., Tomko, K., Willis, M., Kelleher, C., Cloutier, M., Husby, E., Foga, S., Nakamura, H., Platson, M., Wethington, M., Jr., Williamson, C., Bauer, G., Enos, J., Arnold, G., Kramer, W., Becker, P., Doshi, A., D'Souza, C., Cummens, P., Laurier, F., Bojesen, M., 2018, "ArcticDEM", <https://doi.org/10.7910/DVN/OHHUKH>, Harvard Dataverse, V1, [2022-05-20].
- Pye, K. and Tsoar, H., 1987. The mechanics and geological implications of dust transport and deposition in deserts with particular reference to loess formation and dune sand diagenesis in the northern Negev, Israel. *Geological Society, London, Special Publications*, 35(1), pp.139-156.
- Schillereff, D.N., Chiverrell, R.C., Sjöström, J.K., Kylander, M.E., Boyle, J.F., Davies, J.A., Toberman, H. and Tipping, E., 2021. Phosphorus supply affects long-term carbon accumulation in mid-latitude ombrotrophic peatlands. *Communications Earth & Environment*, 2(1), pp.1-10.
- Schofield, J.E., Edwards, K.J., Mighall, T.M., Cortizas, A.M., Rodríguez-Racedo, J. and Cook, G., 2010. An integrated geochemical and palynological study of human impacts, soil erosion and storminess from southern Greenland since c. AD 1000. *Palaeogeography, Palaeoclimatology, Palaeoecology*, 295(1-2), pp.19-30.
- Sernander, R., 1908. On the evidences of postglacial changes of climate furnished by the peat-mosses of Northern Europe. *Geologiska Föreningen i Stockholm Förhandlingar*, 30(7), pp.465-473.
- Sharma, S., Singh, R. and Nielson, G.G., 1983. Selenium in soil, plant, and animal systems. *Critical Reviews in Environmental Science and Technology*, 13(1), pp.23-50.
- Shaw, P.D. and Hager, L.P., 1959. An enzymatic chlorination reaction. *Journal of the American Chemical Society*, 81(4), pp.1011-1012.
- Shotyk, W., 1997. Atmospheric deposition and mass balance of major and trace elements in two oceanic peat bog profiles, northern Scotland and the Shetland Islands. *Chemical Geology*, 138(1-2), pp.55-72.
- Shotyk, W., Cheburkin, A.K., Appleby, P.G., Fankhauser, A. and Kramers, J.D., 1997. Lead in three peat bog profiles, Jura Mountains, Switzerland: enrichment factors, isotopic composition, and chronology of atmospheric deposition. *Water, Air, and Soil Pollution*, 100(3), pp.297-310.

- Shotyk, W., Chen, B. and Krachler, M., 2005 (b). Lithogenic, oceanic and anthropogenic sources of atmospheric Sb to a maritime blanket bog, Myrarnar, Faroe Islands. *Journal of Environmental Monitoring*, 7(12), pp.1148-1154.
- Shotyk, W., Goodsite, M.E., Roos-Barracough, F., Givelet, N., Le Roux, G., Weiss, D., Cheburkin, A.K., Knudsen, K., Heinemeier, J., van Der Knaap, W.O. and Norton, S.A., 2005 (a). Accumulation rates and predominant atmospheric sources of natural and anthropogenic Hg and Pb on the Faroe Islands. *Geochimica et Cosmochimica Acta*, 69(1), pp.1-17.
- Shotyk, W., Krachler, M., Martínez Cortizas, A., Cheburkin, A.K. and Emons, H., 2002. A peat bog record of natural, pre-anthropogenic enrichments of trace elements in atmospheric aerosols since 12 370 14C yr BP, and their variation with Holocene climate change. *Earth and Planetary Science Letters*, 199(1-2), pp.21-37.
- Shotyk, W., Weiss, D., Kramers, J.D., Frei, R., Cheburkin, A.K., Gloor, M. and Reese, S., 2001. Geochemistry of the peat bog at Etang de la Gruère, Jura Mountains, Switzerland, and its record of atmospheric Pb and lithogenic trace metals (Sc, Ti, Y, Zr, and REE) since 12,370 14C yr BP. *Geochimica et Cosmochimica Acta*, 65(14), pp.2337-2360.
- Sjöström, J.K., Bindler, R., Granberg, T. and Kylander, M.E., 2019. Procedure for organic matter removal from peat samples for XRD mineral analysis. *Wetlands*, 39(3), pp.473-481.
- Sjöström, J.K., Bindler, R., Martínez Cortizas, A., Björck, S., Hansson, S.V., Karlsson, A., Ellerton, D.T. and Kylander, M.E., 2022. Late Holocene peat paleodust deposition in south-western Sweden-exploring geochemical properties, local mineral sources and regional aeolian activity. *Chemical Geology*, 602, p.120881.
- Sjöström, J.K., Martínez Cortizas, A., Hansson, S.V., Sánchez, N.S., Bindler, R., Rydberg, J., Mörth, C.M., Ryberg, E.E. and Kylander, M.E., 2020. Paleodust deposition and peat accumulation rates—Bog size matters. *Chemical Geology*, 554, p.119795.
- Steinmann, P. and Shotyk, W., 1997. Chemical composition, pH, and redox state of sulfur and iron in complete vertical porewater profiles from two Sphagnum peat bogs, Jura Mountains, Switzerland. *Geochimica et Cosmochimica Acta*, 61(6), pp.1143-1163.
- Stewart, H., Bradwell, T., Bullard, J., Davies, S.J., Golledge, N. and McCulloch, R.D., 2017. 8000 years of North Atlantic storminess reconstructed from a Scottish peat record: implications for Holocene atmospheric circulation patterns in Western Europe. *Journal of Quaternary Science*, 32(8), pp.1075-1084.
- Sverrisdottir, G., 2007. Hybrid magma generation preceding Plinian silicic eruptions at Hekla, Iceland: evidence from mineralogy and chemistry of two zoned deposits. *Geological Magazine*, 144(4), pp.643-659.
- Tarnocai, C. and Stolbovoy, V., 2006. Northern peatlands: their characteristics, development and sensitivity to climate change. *Developments in earth surface processes*, 9, pp.17-51.

- Tierney, J.J. ed., 1967. *Liber de Mensura Orbis Terrae* (Vol. 6). Dublin Institute for Advanced Studies.
- Turney, C.S., 1998. Extraction of rhyolitic component of Vedde microtephra from minerogenic lake sediments. *Journal of Paleolimnology*, 19(2), pp.199-206.
- Vickers, K., Bending, J., Buckland, P.C., Edwards, K.J., Hansen, S.S. and Cook, G., 2005. Toftanes: The paleoecology of a Faroese Landnám farm. *Human Ecology*, 33(5), pp.685-710.
- Vitt, D.H., 2006. Functional characteristics and indicators of boreal peatlands. In *Boreal peatland ecosystems*. Springer, Berlin, Heidelberg, pp. 9-24.
- Wastegård, S., 2002. Early to middle Holocene silicic tephra horizons from the Katla volcanic system, Iceland: new results from the Faroe Islands. *Journal of Quaternary Science: Published for the Quaternary Research Association*, 17(8), pp.723-730.
- Wastegård, S. and Davies, S.M., 2009. An overview of distal tephrochronology in northern Europe during the last 1000 years. *Journal of Quaternary Science: Published for the Quaternary Research Association*, 24(5), pp.500-512.
- Wastegård, S., Björck, S., Grauert, M. and Hannon, G.E., 2001. The Mjáuvøtn tephra and other Holocene tephra horizons from the Faroe Islands: a link between the Icelandic source region, the Nordic Seas, and the European continent. *The Holocene*, 11(1), pp.101-109.
- Wastegård, S., Gudmundsdóttir, E.R., Lind, E.M., Timms, R.G., Björck, S., Hannon, G.E., Olsen, J. and Rundgren, M., 2018. Towards a Holocene tephrochronology for the Faroe Islands, north Atlantic. *Quaternary Science Reviews*, 195, pp.195-214.
- Weiss, D., Shotyk, W., Appleby, P.G., Kramers, J.D. and Cheburkin, A.K., 1999. Atmospheric Pb deposition since the industrial revolution recorded by five Swiss peat profiles: enrichment factors, fluxes, isotopic composition, and sources. *Environmental Science & Technology*, 33(9), pp.1340-1352.
- Wieder, R.K., Vitt, D.H. and Benscoter, B.W., 2006. Peatlands and the boreal forest. In *Boreal peatland ecosystems*. Springer, Berlin, Heidelberg. pp. 1-8.
- Woillard, G.M., 1978. Grande Pile peat bog: a continuous pollen record for the last 140,000 years. *Quaternary Research*, 9(1), pp.1-21.
- Woollings, T. and Blackburn, M., 2012. The North Atlantic jet stream under climate change and its relation to the NAO and EA patterns. *Journal of Climate*, 25(3), pp.886-902.
- Yeloff, D. and Mauquoy, D., 2006. The influence of vegetation composition on peat humification: implications for palaeoclimatic studies. *Boreas*, 35(4), pp.662-673.
- Zaccone, C., Coccozza, C., Shotyk, W. and Miano, T.M., 2008. Humic acids role in Br accumulation along two ombrotrophic peat bog profiles. *Geoderma*, 146(1-2), pp.26-31.
- Zobel, D.B. and Antos, J.A., 1997. A decade of recovery of understory vegetation buried by volcanic tephra from Mount St. Helens. *Ecological Monographs*, 67(3), pp.317-344.

Zhang, X., Walsh, J.E., Zhang, J., Bhatt, U.S. and Ikeda, M., 2004. Climatology and interannual variability of Arctic cyclone activity: 1948–2002. *Journal of climate*, 17(12), pp.2300-2317.

Appendix

A. Age-Depth Model

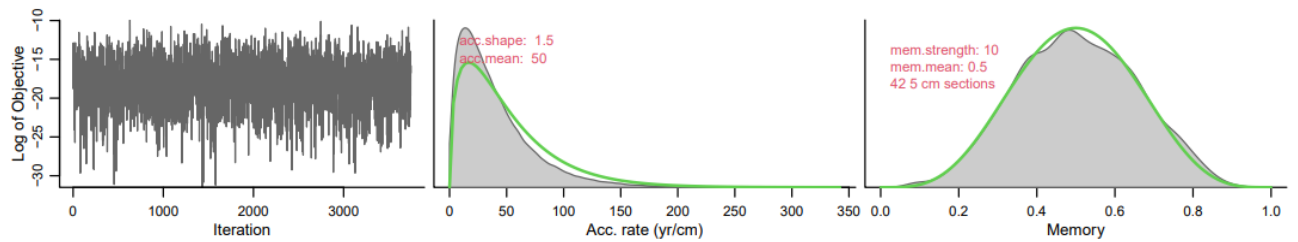


Figure A1. Markov Chain Monte Carlo iterations and prior (green) and posterior (grey) distributions of growth rate and memory.

Table A1. Age-depth model settings.

Description	Setting	Value
Minimum depth	#d.min	0
Maximum depth	#d.max	202
Depth Interval	#d.by	1
Mean of growth rate gamma distribution	#acc.mean	50
Shape of growth rate gamma distribution	#acc.shape	1.5
Memory mean	#mem.mean	0.5
Memory strength	#mem.strength	10
Depth of any hiatuses	#hiatus.depths	NA
Time scale (0=cal yr BP and 1= BC/AD)	#BCAD	0
Calibration curve (1=IntCal20)	#cc	1
Postbomb curve (0=default)	#postbomb	0
Depth unit	#depth.unit	cm
Age unit	#age.unit	yr
Distribution of dates (0=student-t distribution)	#normal	0
Distribution parameter a	#t.a	3
Distribution parameter b	#t.b	4
Core-wide age offset (default 0)	#delta.R	0
Core-wide age offset standard deviation (default 0)	#d.STD	0
Probability	#prob	0.95

B. Individual Element Profiles

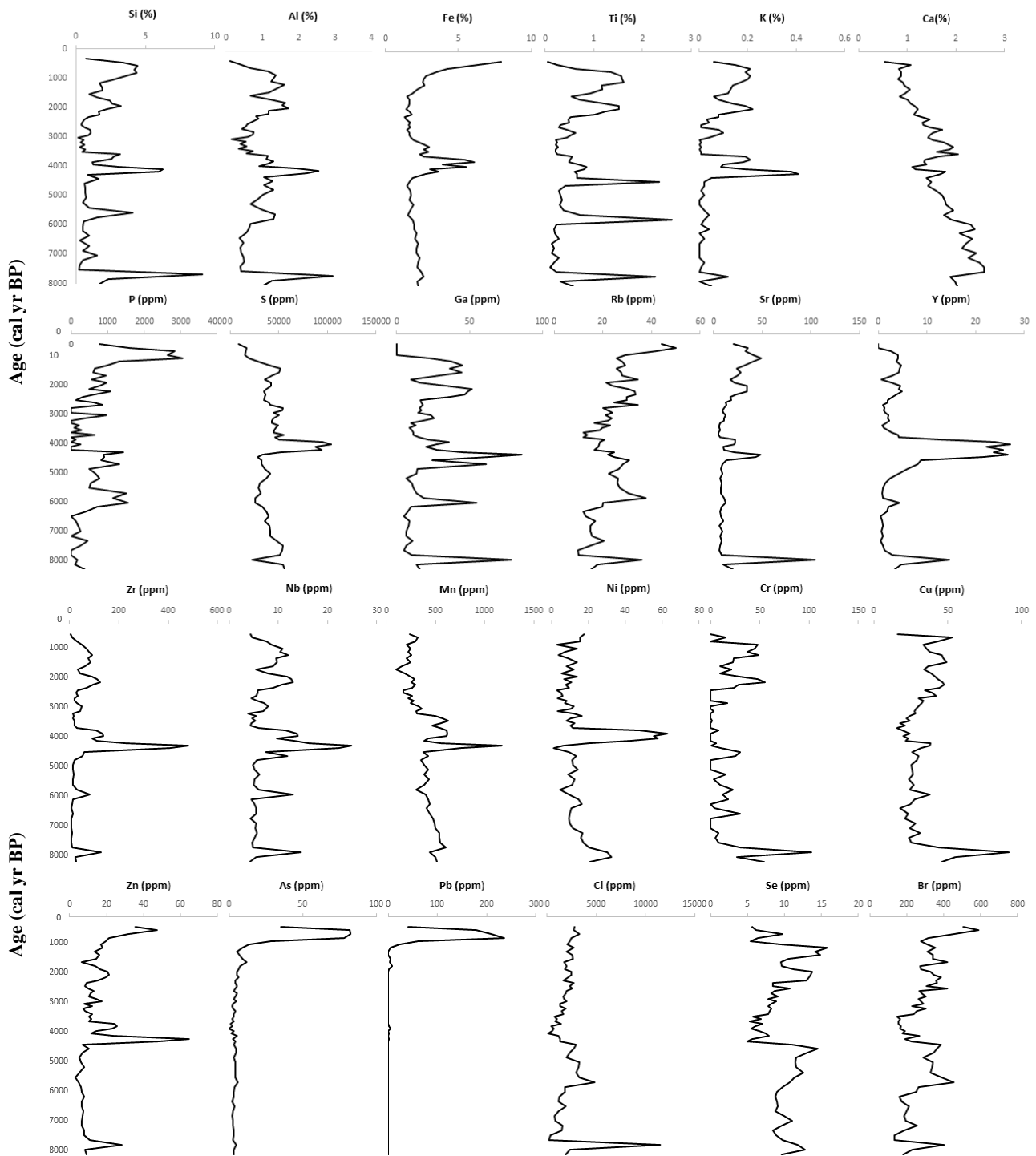


Figure B1. Elemental concentrations from WD-XRF plotted against age.

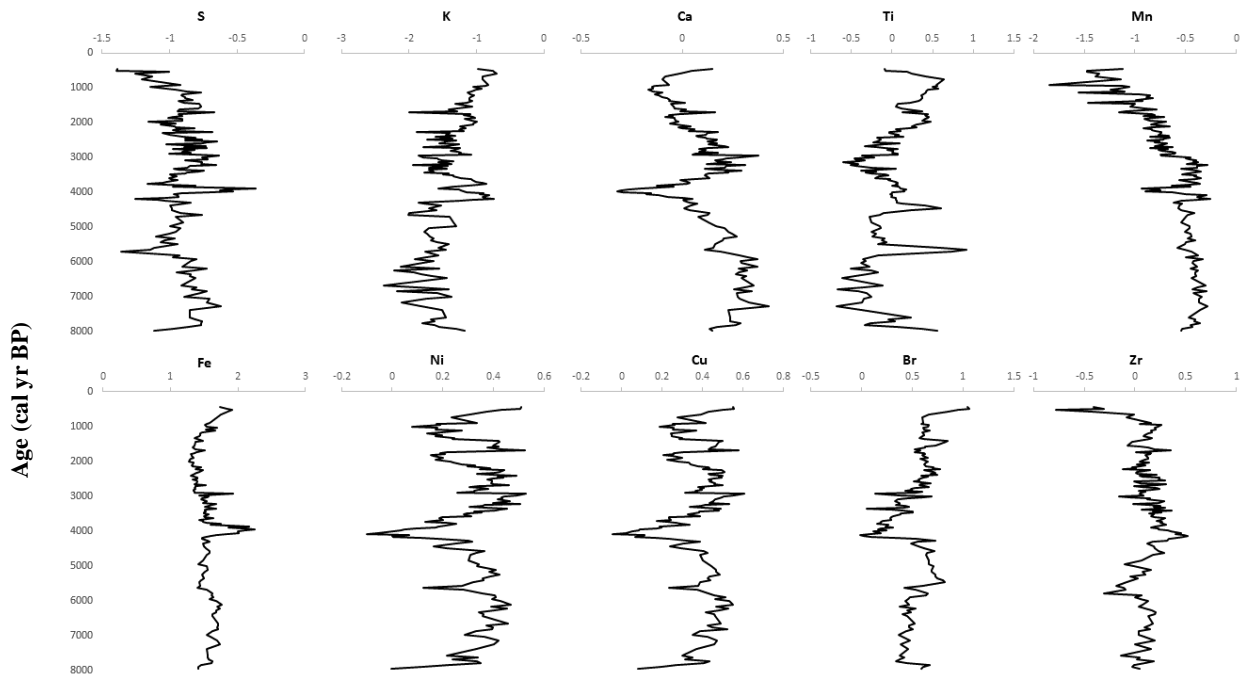
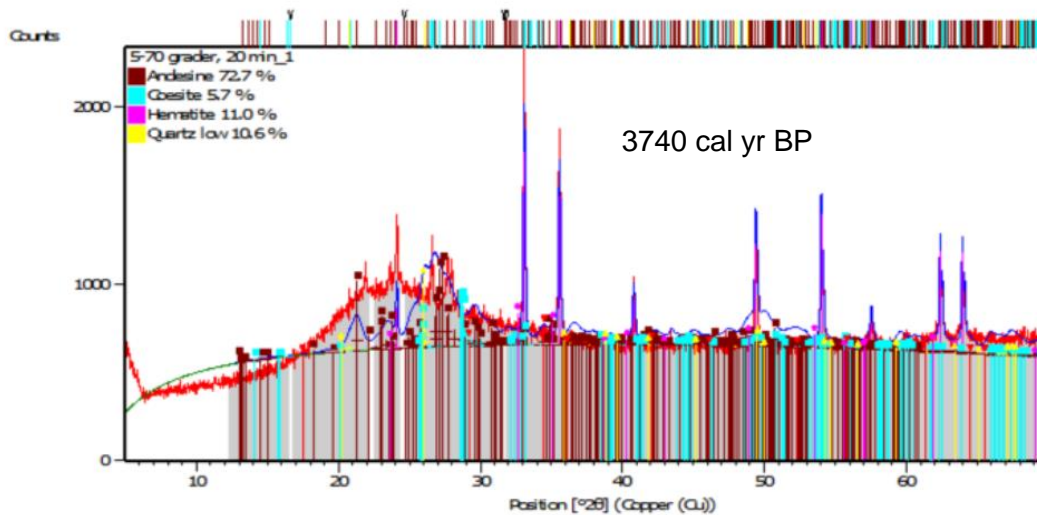
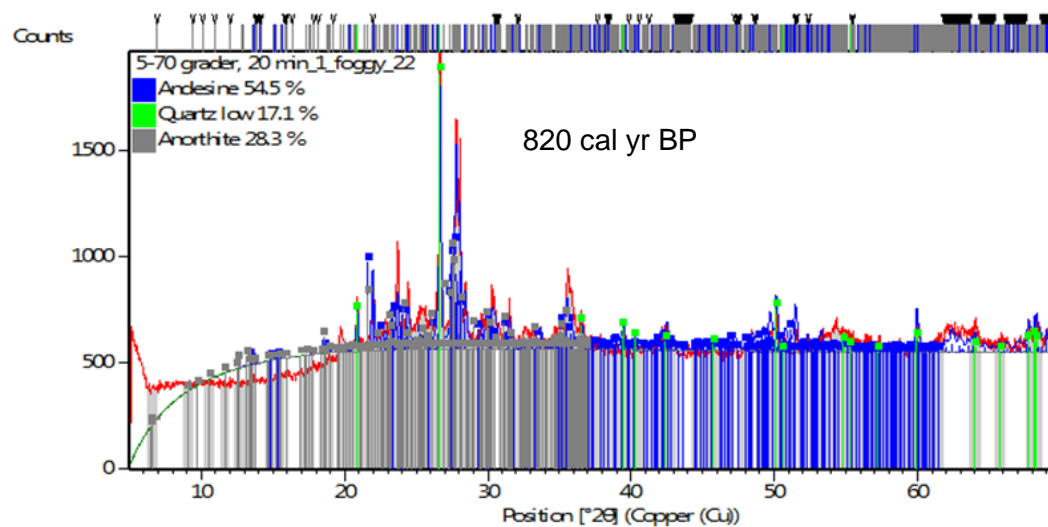
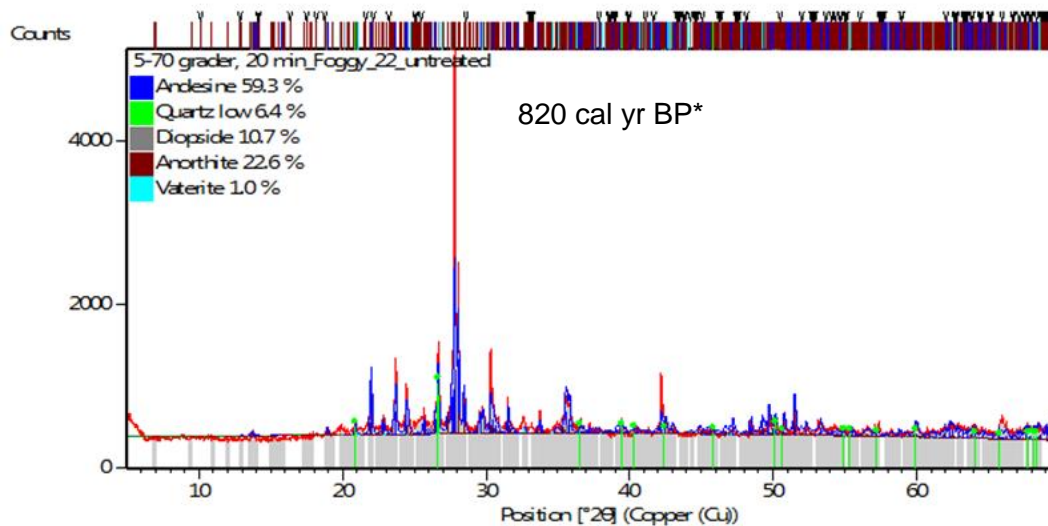


Figure B2. Centred log ratio (clr) transformed peak areas with zeroes removed from XRF core scanning.

C. XRD-Diffractograms



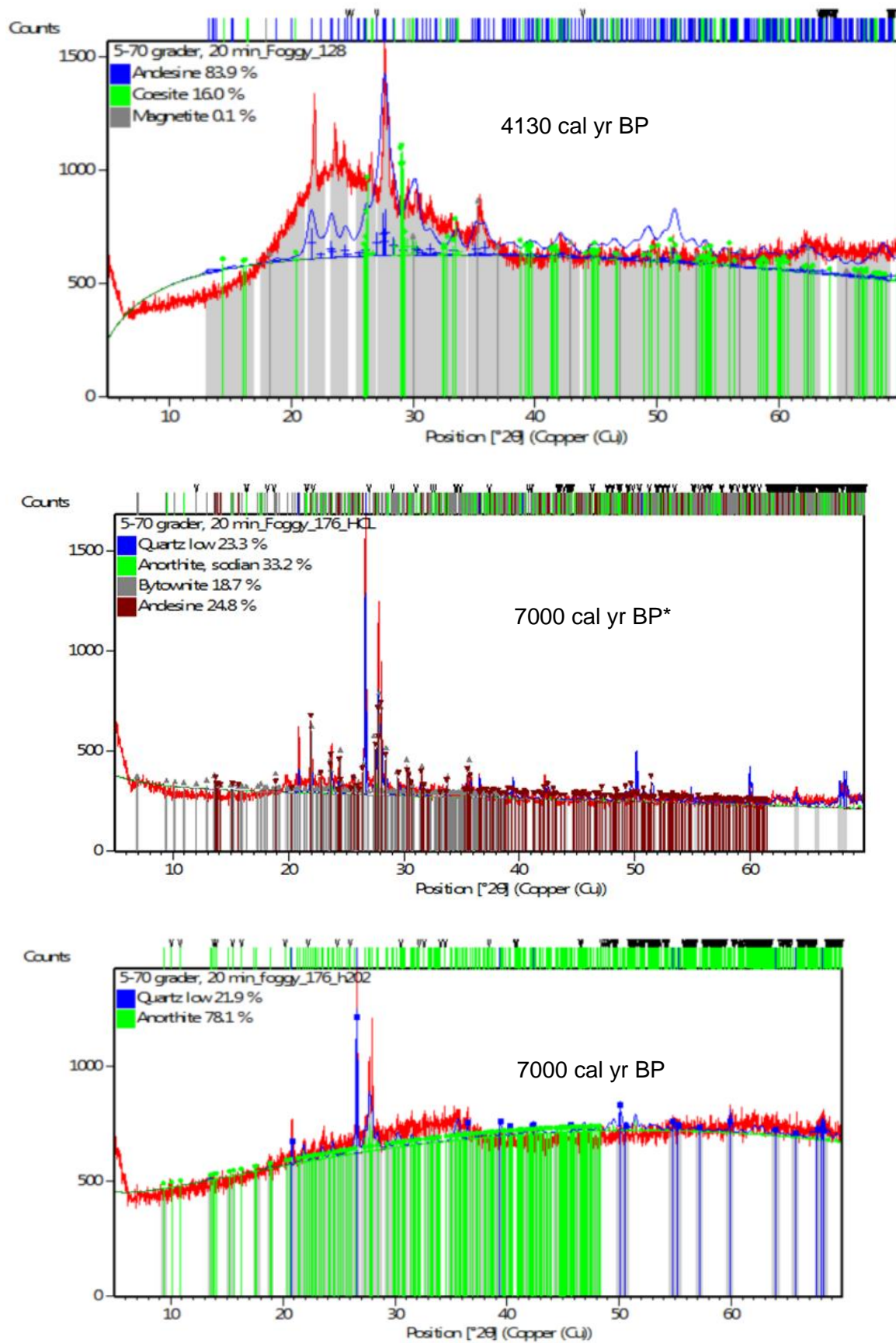


Figure C1. Diffractograms from XRD analysis. `** denotes samples not treated with H₂O₂.